Q19990728000Z

Infiltration Abstractions for Shallow Soil Over Fractured Bedrock in a Semiarid Climate

Stuart A. Stothoff
Stothoff Environmental Modeling
1206 La Rue Street
Houston, TX 77019, USA

Abstract

Deep percolation of water is consistently identified as critical to the performance of the proposed repository at Yucca Mountain, Nevada. In turn, simulations of deep percolation depend on appropriate surface boundary conditions. An investigation of factors influencing mean annual infiltration at Yucca Mountain under present-day conditions and possible future-climate conditions is presented here. Two situations are considered, deep (semi-infinite) alluvium and shallow colluvium (collectively called soil or cover) overlying bedrock or a fracture continuum within an impermeable matrix. A series of one-dimensional bare-soil (i.e., without consideration of transpiration) simulations of the near-surface environment, using a decade of measured hourly meteorological boundary conditions representative of the semiarid Yucca Mountain area, is used to examine mean annual infiltration by varying one or more factors in the different simulations. Sensitivities to meteorological factors are discussed for both the deep and shallow situations. The simulations are too short to include infrequent large events, so that the estimate may not be a true mean annual average, but the sensitivities should be reasonably representative. Based on the set of one-dimensional simulations, abstractions are presented relating bare-soil mean annual infiltration to soil and fracture hydraulic properties, mean annual meteorologic inputs, and cover thickness. Mean annual infiltration responds exponentially to climate change and is more sensitively affected under low-infiltration conditions. Net infiltration is strongly affected by the cover thickness over the fractured bedrock; as cover thickness increases, net infiltration decreases but becomes more sensitive to meteorologic changes. Mean annual infiltration is also strongly affected by soil texture; as the texture becomes finer, net infiltration decreases. The exponential response of net infiltration to climate change suggests that cumulative net infiltration may be underestimated unless perturbations in the climate cycle are considered. Further, mean annual infiltration will have more complex behavior over a glacial cycle when the response of mean annual infiltration to changes in soil thickness is considered as well as the response to meteorologic factors. Soil texture and thickness also respond to climate change and are unlikely to stay in equilibrium with the climate.

1 INTRODUCTION

Performance assessments of the high-level waste repository proposed for Yucca Mountain (YM), Nevada, consistently identify moisture levels at the repository horizon and moisture fluxes passing through the repository horizon as critical factors in the ability of the proposed repository to isolate waste from the environment [*Nuclear Regulatory Commission*, 1992; *Nuclear Regulatory Commission*, 1995; *Sandia National Laboratories*, 1992; *Sandia National Laboratories*, 1994; *TRW*, 1995; *Electric Power Research Institute*, 1990; *Electric Power Research Institute*, 1992; *Electric Power Research Institute*, 1996]. As moisture fluxes at the repository level depend on the net moisture entering the mountain through infiltration, and as the climate at the YM site has changed and will change over the time scales of regulatory interest, multiple lines of investigation must be used to bound the moisture fluxes expected at the repository, including measurements of current near-surface infiltration rates and deep moisture fluxes, numerical simulations of moisture redistribution, and indirect measurements of long-term infiltration rates.

Infiltration in the YM region has been examined extensively. Site- and regional-scale estimates of recharge were made by *Czarnecki* [1985] and *Montazer and Wilson* [1984]. *Flint and Flint* [1994] presented a preliminary estimate of the spatial distribution of flux in the YM region, based primarily on measured matrix properties. Other detailed modeling and conceptual exercises examining shallow infiltration processes have been performed by *Hevesi and Flint* [1993], *Flint et al.* [1993], *Hevesi et al.* [1994], *Flint et al.* [1994], *Flint et al.* [1996a], *Long and Childs* [1993], *Hudson et al.* [1994], *Kwicklis et al.* [1994], *Stothoff et al.* [1995], *Stothoff et al.* [1996], *Stothoff et al.* [1997], *Woolhiser et al.* [1997], and *Woolhiser et al.* [1999].

The shallow-infiltration modeling exercises have typically been limited to one-dimensional (1D) models, with two-dimensional (2D) radial models applied to particular infiltration experiments. A trend developing in the literature suggests that the water balance in the repository footprint at YM is not dominated by infiltration in washes, where conventional wisdom might place peak infiltration rates, but rather is dominated by infiltration in the low-permeability but densely fractured welded tuffs cropping out at ridgetops and sideslopes. As the trend has developed, estimates of areally averaged infiltration have been raised to as much as 25 mm/yr (roughly 15 percent of mean annual precipitation (MAP)), based on a network of 99 neutron probes [*Flint et al.*, 1995]. Numerous indirect lines of evidence, including chloride mass balance calculations, thermal-flux discrepancy calculations, and perched-water-body volume balance calculations, are interpreted by the Department of Energy to suggest that areal-average mean annual infiltration (MAI) in the repository footprint is roughly 1 to 10 mm/yr [*Bodvarsson and Bandurraga*, 1996; *Bodvarsson et al.*, 1997]. Using the available data, *Winterle et al.* [1999] provides an estimate of the upper bound for areal-average MAI of roughly 25 mm/yr.

Estimates of total channel infiltration during runoff events in the adjacent Solitario Canyon watershed are 12 to 38 mm/yr in the channel system [*Woolhiser et al.*, 1999]. Distributed over the watershed, however, the estimates are on the order of 0.18 to 0.57 mm/yr, and these estimates represent an upper bound for MAI as evapotranspiration is not considered. Although the large fluxes resulting from channel infiltration may provide a mechanism for local fast pathways, the water balance suggests that channel infiltration may not form a large component of overall net infiltration relative to distributed infiltration.

The study presented here uses numerical simulations to examine the influence of hydraulic properties and climatic variation on MAI at YM. The primary motivation of the study is to provide insight into the boundary conditions that might be appropriate for simulations of flow in the deep subsurface. In this paper, numerous detailed 1D simulations are abstracted into a response function for MAI as a function of hydraulic properties, mean annual meteorologic inputs, and depth of surficial cover. Conclusions are then drawn regarding the relative influence of the various inputs on estimates of MAI. Further, the influence of variability and parameter uncertainty on the expected value of MAI is assessed using first-order and Monte-Carlo techniques. The exponential response of MAI to changes in input parameters is shown to increase expected values of MAI as uncertainty and variability increases, with larger response occurring under conditions of smaller MAI.

The response function is only appropriate for relatively small areas, three to five orders of magnitude smaller than the YM repository footprint. Guidance on the spatial and temporal distribution of MAI at the heterogeneous YM site has been obtained using a response function for MAI in conjunction with a digital elevation model (DEM) [*Stothoff et al.*, 1995; *Stothoff et al.*, 1996; *Stothoff and Sagar*, 1997; *Coleman et al.*, 1998] and the combination has even been used in performance assessment [*Mohanty and McCartin*, 1998]. When a DEM is available for the site and all of the required input parameters are mapped to the pixels of the DEM, MAI can be estimated for each pixel with areal averages obtained by summing over all pixels. The analyses presented here also may be easily repeated for each pixel to provide a more global estimate of uncertainty. The breadth of hypotheses regarding site conditions that can be tested using the response-function approach is far wider than could be achieved with the same computational effort using 2D or three-dimensional (3D) models. Nevertheless, the approach is questionable for regions where lateral flow may strongly influence vertical flow, as may occur locally at YM (*e.g.*, ridgetops, wash channels, at the foot of slopes). Estimates of spatial distributions of MAI at YM using the response-function approach will be discussed in a forthcoming paper.

The overall approach of abstracting numerous detailed 1D simulations into a response function for MAI, then using information regarding the functional inputs to estimate MAI, has the advantage of allowing extremely fast turnaround for screening exercises and sensitivity tests once the response function is available. For example, total computational time necessary to reproduce all analyses presented herein, aside from the detailed 1D simulations, is on the order of minutes on a Sun Sparc-20 workstation. In comparison, one detailed 1D simulation used to develop the abstraction can take several hours to weeks to complete on the same workstation.

A description of the site is presented in Section 2. Using a 1D nonisothermal simulator, BREATH [*Stothoff*, 1995], a series of representative simulations was run with various soil thicknesses, systematically varying hydraulic and meteorologic parameters. Results from these simulations are discussed in Section 3. Abstractions of the functional dependence of bare-soil MAI to these parameters are presented in Section 4. Predictions of the abstraction are discussed in Section 5. Finally, implications for changes in MAI over a glacial cycle are examined in Section 6, using several typical cases.

2 SITE DESCRIPTION

A location map of the YM repository footprint, based on the *Day et al.* [1998] geologic map, is shown in Figure 1. The smaller eastern portion of the footprint is optional and may not be used. All units cropping out in the repository footprint are ash-fall tuffs with various degrees of welding. In Figure 1, the units are grouped into (i) alluvium and colluvium (30 percent of the area in the figure), (ii) caprock (10 percent), (iii) moderately to densely welded zones (55 percent), and (iv) non to partially welded zones (5 percent). Alluvium depths are less than 10 m and generally less than 5 m over the repository footprint. The caprock region features relatively large moderately welded blocks with distinct wide soil-filled joints. Densely welded nonlithophysal zones are distinguished by significantly heavier fracture densities than the other moderately to densely welded zones and perhaps less precipitant in-fillings. Above the repository footprint, nonwelded zones are only exposed on the steep west flank of Yucca Crest. Bedrock fractures at YM are generally soil-filled or precipitate-filled (carbonate or silicate), but unfilled fractures might occur in any unit and are common in the nonwelded zones [*Sweetkind et al.*, 1996].

Alluvium completely fills lower-wash bottoms. Elsewhere the bedrock (the rock unit immediately below any unconsolidated surficial materials) is covered with a shallow skin of colluvium with scattered local patches of bare bedrock existing along ridgetops and on steep sideslopes. For simplicity, alluvium and colluvium often will be generically referred to as soil. Rock immediately underlying soil will be referred to as bedrock. At the bottom of slopes, colluvium may collect to greater than 1 m in thickness. The fine portion of the colluvium, and perhaps in the uppermost alluvial layer, is predominantly æolian-derived, with rather uniform grain-size distributions across the repository block representative of sandy loam (*Schmidt* [1989]; personal communication, D. Or, 1997, 1998). Some slopes feature loose talus, with the interstices partially to completely filled with fine æolian dust. Channels in the alluvial terraces may not contact bedrock directly; channels in the upper washes tend to be incised into bedrock, and exposed fractures in these channels may be filled with fine sediment.

Based on preliminary observations, the caprock region features large (0.5 to 2 m) moderately welded blocks with distinct wide (5 to 15 cm) fissures. Carbonate coatings are present along the bedrock surface in some locations, but the fractures tend to be primarily soil-filled. Soil cover can be nonexistent to locally more than 0.7 m thick, although limited observation suggests that typical thicknesses are roughly 30 cm. The caprock region is considered herein to be modeled as a soil continuum above a soil-filled fracture continuum.

Above the repository footprint, nonlithophysal densely welded units are almost exclusively exposed on steep sideslopes. Soils are nonexistent to tens of centimeters, and streaks of talus may be present. In the nonlithophysal zones, fractures or joints are typically spaced on the order of tens of centimeters; rock fragments derived from this zone are angular and sharp-edged. Based on personal observation, the joints appear relatively free of carbonates compared to the other densely welded zones, and in some locations fractures gape open. There is some question about whether the fracture fillings in the nonlithophysal zones should be modeled as soil-filled or carbonate-filled. The relative lack of carbonate fillings in the nonlithophysal zone, at least at the soil/bedrock interface, suggests that enough water may percolate through the fracture system to keep the carbonates dissolved. If so, carbonate fillings may begin to appear at depth; however, the relative lack of near-surface carbonate fillings suggests that infiltration may be significant in the nonlithophysal zone. The nonlithophysal-zone fractures are considered soil-filled for modeling herein.

In the other densely welded zones, the cooling-joint fractures have smaller apertures, are more widely spaced, and tend to be filled with carbonates or silicates, particularly on south-facing slopes. Drill-pad exposures suggest that the fillings extend for roughly a meter into the bedrock. These zones are modeled herein as consisting of a soil continuum above a carbonate-filled fracture continuum.

In the current study, the shallow YM infiltration system is conceptualized as one of two limiting cases: (i) deep (effectively semi-infinite) alluvium, typical of washes; and (ii) a shallow skin of alluvium or colluvium, overlying a densely fractured welded bedrock idealized as a fracture continuum within an impermeable matrix. *Stothoff* [1997] suggests (for bare soil above an unfilled-fracture continuum) that the transition between the limiting cases may occur with a soil thickness on the order of 5 to 10 m. Further, in the absence of lateral flow and fast pathways, evaporation alone in the semiarid YM environment is sufficient to eliminate infiltration for thicknesses of fractured-bedrock cover between the transition depth and roughly 25 to 50 cm for many types of soils. The results from the current study are consistent with the previously identified transition depth. However, it is found that the hydraulic behavior of filled fractures is sufficiently different from unfilled fractures that, in the absence of transpiration, significant MAI may occur for all soil thicknesses.

3 SHALLOW INFILTRATION SIMULATIONS

By performing a sufficient number of simulations of the flow of moisture and energy in a 1D column representative of the shallow surface of YM, while changing hydraulic parameters and meteorologic inputs in a systematic way, it is possible to construct a response surface for the variation of MAI with the input values. Determination of a response surface through systematic variation of parameters may be most useful when simulations use parameters at or beyond the extremes of their likely range, particularly when the sensitivity to that parameter is low. Then, assessment of responses for lesser changes can be accomplished through interpolation rather than extrapolation. However, individual simulations often use a parameter set not representative of any particular porous medium, particularly as correlation between properties is ignored. This section discusses the simulations used to construct the response surface.

The BREATH simulator used in the study considers the coupled flow of moisture and energy in a porous medium, as described in detail by *Stothoff* [1995]. The sensitivity of net long-term infiltration estimates to hydraulic properties, using BREATH, was considered by *Stothoff* [1997]. Following the procedures in *Stothoff* [1997], two types of simulations are considered: (i) semi-infinite columns of alluvium, and (ii) columns of shallow colluvium overlying a semi-infinite fracture or bedrock continuum. At the bottom of the column, the gradients of saturation and temperature are assumed to be zero, allowing gravity drainage of water and advective losses of energy. In all cases, the semi-infinite behavior is approximated by using columns deep enough that the bottom boundary conditions have minimal impact on the estimated net infiltrations. A domain of 30 m in depth is assumed sufficient to achieve this goal for the hydraulic and thermal properties considered. It is recognized, however, that it is unlikely for fractures to be filled to a depth of 30 m.

All simulations are driven using the same sequence of 10 yr of hourly meteorologic events, based on hourly readings from the Desert Rock, NV, National Weather Service meteorologic station located approximately 30 miles to the east of YM [*National Climatic Data Center*, 1994b]. Procedures for converting the National Weather Service readings into BREATH meteorological inputs are discussed by *Stothoff* [1997]. The meteorological record runs from March 1, 1983, through February 28, 1993; the sequence was the longest available for this station at the onset of the study with all the meteorologic inputs measured at hourly intervals. The sequence is repeated until the effects of the initial conditions are eliminated. Centuries are required to eliminate initial conditions in deep-alluvium, low-MAI cases, but the initial conditions dissipated in the first cycle for all of the fracture-continuum simulations. The response surface is based on the last decade of the simulations. One decade may be too short of a time period to capture the full range of precipitation events in a statistically robust way; however, this is sufficiently long to gain considerable insight into the changes in behavior that might be expected with different hydraulic properties and climatic regimes.

To investigate the effects of climatic change, individual simulations may modify the Desert Rock sequence to capture climatic change by scaling (all input factors but air temperature) or shifting (air temperature) all hourly readings. No modified sequence is likely to be representative of actual climate change, as climatic factors do not necessarily change independently and seasonality changes are not considered; however, the general response of MAI to the individual factors can be assessed using this approach.

Whenever precipitation exceeds infiltration, the excess is assumed to run off and overland flow is not considered further. Lateral subsurface flow is not considered. These two assumptions would tend to yield MAI estimates that are too large at the top of slopes and too small at the bottom of slopes, but may not be unreasonable for midslope regions.

Within 24 hours of a precipitation event, hourly meteorological readings are used; otherwise, moving monthly average readings are used. Adaptive time stepping is used to ensure mass balance, with a maximum time step of 1 hr. During rainfall events, a single hour may take several hundred time steps.

3.1 Semi-Infinite Column Simulations

To examine the impact on MAI in deep alluvium, two homogeneous alluvium columns are considered, using a high-permeability (intrinsic permeability $k = 10^{-5}$ cm^2) and a medium-permeability ($k = 10^{-8}$ cm^2) alluvium. For each column considered, porosity is 0.3, van Genuchten m is 0.2, and van Genuchten α is 10^{-3} Pa^{-1}. The 30-m column is discretized with 51 nodes, with a top element of 2 cm and each successive element increasing in length by 10 percent. Both alluvium cases were considered by *Stothoff* [1997], who found that, for a similar semi-infinite column with all parameters held constant (aside from permeability), as permeability increases from 10^{-5} cm^2 to 10^{-10} cm^2, MAI increases to a peak value with permeability at roughly 10^{-8}, then drops precipitously to essentially zero with permeability at 10^{-10} cm^2. Much higher net infiltration occurs for the medium-permeability alluvium than for the high-permeability alluvium due to reduced evaporation.

The base-case simulation for each alluvium uses the Desert Rock meteorological record directly, as was the case for all simulations presented by *Stothoff* [1997]. To identify first-order sensitivities to inputs, additional simulations are run for each column, systematically perturbing one of the meteorologic inputs about the base-case value. A similar procedure was followed by *Stothoff* [1997] to examine the effect of hydraulic properties on MAI.

The long-term net infiltration rate resulting from each simulation is plotted in Figure 2, where the perturbation for most weather parameters is obtained by uniformly scaling each hourly value for the parameter. Temperatures, however, are perturbed by adding a constant value to all hourly temperature values. Simulations with incident solar radiation arising from a ground rotation of 30 degrees east, west, north, and south are denoted Angle in Figure 2. Relative changes in MAI for the same perturbation in the meteorologic input parameter are roughly twice as great in the low-MAI (high-permeability) column than in the high-MAI (medium-permeability) column.

In Figure 3, MAI is plotted as a function of the mean annual moisture content below the wetting-pulse perturbation depth for the same set of simulations. Conditions at depth are almost steady state in these simulations, so that the direct link between flux and saturation provided by the relative permeability function provides the strong correlation between MAI and moisture content seen in Figure 3. Most points arise from simulations that modify evaporation-affecting parameters. The remaining points, from modified-precipitation simulations, align with the evaporation-affecting results. Interestingly, multiplying MAI by $k^{0.55}$ and dividing each moisture content by the corresponding base-case moisture content yields curves that are aligned. Note that scaling by $k^{0.5}$ is appropriate for a diffusion-dominated system. Similar exercises with a shallow layer overlying a deeper layer have different slopes for modified-precipitation and modified-evaporation simulations.

Meteorological factors have less impact on MAI in deep alluvium than do the hydraulic properties examined by *Stothoff* [1997], hence identifying the hydraulic properties of alluvium is overall more significant to identifying MAI in deep alluvium at YM. Nevertheless, systematic trends in the meteorologic variables (*i.e.*, due to elevation variation or climatic change) can yield systematic variation in MAI. Elevation variation at YM results in small but systematic variability in MAP, mean annual temperature (MAT), and mean annual vapor density (MAV), while slope aspect effects (*e.g.*, north-facing slopes versus south-facing slopes) result in systematic variability in mean annual net incoming radiation (MAR) through variability in incident shortwave radiation. Protection from prevailing winds occurs in the YM washes, systematically varying mean annual windspeed (MAW); surface roughness also changes from location to location due to variation in vegetation and soil composition, with a similar effect. Significant variation in both MAP and MAT should occur due to climatic change, with perhaps some change in MAV and cloud cover (with concomittant impact on incoming radiation) as well. Changes in vegetation density would change surface roughness, thereby changing effective MAW. Of these factors, MAP and MAT would appear to have the most significant impacts on the spatial distribution of MAI, a point that will be demonstrated in Section 5.1.

3.2 Shallow Soil Over Fractured Bedrock Simulations

The fractures at the top of the bedrock at YM are typically unfilled, filled with soil, or filled with precipitants (*e.g.*, carbonate or silicaceous material). The response of distributed MAI to increasing bare-soil cover above an unfilled fracture continuum was examined by *Stothoff* [1997]. He found that for the base-case soil examined herein, MAI dropped sharply with increasing cover, decreasing to zero with only a fraction of a meter of cover and staying at zero for soil depths up to almost 10 m. However, once the soil cover reached 10 m, the medium was essentially semi-infinite and MAI reached about one percent of MAP (depending on soil properties). The increase in soil depth was accompanied by a monotonic increase in mean annual moisture content at the soil/fracture interface, reaching essentially saturated conditions with 10 m of cover. The nonmonotonic behavior for MAI is explained by the capillary barrier represented by the unfilled fracture; the soil immediately above the fracture must be essentially saturated before the fracture begins to flow. Saturation occurs through wetting pulses (shallow case) or near-perched conditions (deep case). Of course, the addition of shrubs would likely change the picture for deeper soils by retrieving some or all of the moisture that would otherwise penetrate to depth.

Following the same procedure as was followed by *Stothoff* [1997], additional simulations were run using hydraulic properties for the fracture continuum that are more representative of soils or carbonates. Note that the assumption of a fracture continuum in a 1D context tacitly implies that lateral redistribution in the soil is sufficiently rapid to not limit exchange between the soil and the fracture system. Elements at the ground surface were about 1 mm in length, with a minimum of 20 soil elements and 30 fracture elements. These simulations assume that the fracture filling is semi-infinite (at least 30 m thick), although typically the fracture fillings might exist for only a few meters. It is anticipated that limited filling depths would yield behavior intermediate between estimates using semi-infinite unfilled fractures and semi-infinite filled fractures.

Simulations with carbonate-filled fractures are more problematic than unfilled fractures, as there are little data on filling properties; simply obtaining samples from the fractures is difficult, particularly for the more fragile samples (which tend to have relatively large permeabilities). Data package GS950708312211.003, prepared by the United States Geological Survey, reports 15 measurements of fracture-fill materials from YM, with 4 measurements parallel to and 11 measurements perpendicular to the fracture. All four parallel measurements have conductivity values in the range of 8×10^{-7} to 3×10^{-6} m/s, while ten of the perpendicular measurements range from less than 10^{-13} to 5×10^{-8} m/s and one is about 10^{-6} m/s. The samples may represent a mixture of carbonate and silicate fillings, and the relatively sparse data set may not be representative of the site as a whole. Accordingly, simulations labeled as carbonate-filled may not use properties representative of actual fillings.

The measurement orientation relative to the fracture orientation may provide rather different values if the carbonates were deposited in layers; the along-fracture conductivity would be expected to be significantly greater than the across-fracture conductivity in such cases. *Flint et al.* [1996a] used a hydraulic conductivity of 5×10^{-7} m/s (permeability is 5.1×10^{-10} cm^2) for carbonates, but does not report retention properties. Based upon the simulations presented by *Stothoff* [1997], bare-soil alluvium with this permeability is in the transition zone between exhibiting significant MAI and having no net infiltration. *Baumhardt and Lascano* [1993] and *Hennessy et al.* [1983] suggest that calcite has a texture of a fine soil. In the simulations reported herein, carbonate retention properties were assumed to be similar to those of clays. Sensitivity of simulation results to the carbonate retention properties is quite small.

The response of MAI to different soil cover thicknesses is presented from four sets of simulations in Figure 4, with the base-case hydraulic properties reported in Table 1. Two sets are repeated from *Stothoff* [1997], the semi-infinite soil and the soil/unfilled-fracture cases. A third set represents a soil-filled fracture, while the fourth set represents a carbonate-filled fracture. The covering-soil hydraulic properties are identical in the four sets. The perturbation and bedrock cases reported in Table 1 are used in Sections 5 and 6.1 for sensitivity studies.

The response to increases in cover thickness is quite different for the unfilled-fracture set than the two sets with fracture fillings; interestingly, however, the soil- and carbonate-filled sets are quite similar despite having somewhat different hydraulic properties. The unfilled-fracture set has tremendous MAI with very shallow cover, as might be expected, but decreases rapidly as the soil cover increases to only a few tens of centimeters. *Stothoff* [1997] found that this behavior was essentially insensitive to the fracture hydraulic properties. The filled-fracture sets have a much gentler decrease in MAI as the soil cover increases. It is expected that MAI for the semi-infinite case would be achieved with soil depth of about 10 m regardless of the filling material, with the soil-filled fracture case dropping monotonically to the limiting rate and the others exhibiting a minimum for some intermediate soil depth.

A fundamental difference between the unfilled and filled sets lies in the air-entry pressure. The air-entry pressure in the unfilled fractures is much smaller than in the soil, so the fractures represent a capillary barrier to the downward percolation of water in the overlying soil (even though the fractures are extremely permeable at saturation) and drainage into the fracture requires essentially saturated conditions in the soil. On the other hand, the filled fractures have air entry pressures no less than in the soil, so that although the filled fractures have a much smaller saturated hydraulic conductivity than the corresponding unfilled fractures, the fillings are not a capillary barrier. Indeed, the carbonate fillings preferentially attract water, consistent with observations for caliche by *Baumhardt and Lascano* [1993] and *Hennessy et al.* [1983].

3.3 Hydraulic Property Changes

Typical responses of MAI to changing soil and fracture-filling hydraulic properties are shown in Figure 5, where one property is varied between runs while all other inputs are held constant. The base-case simulation set represents the bare soil over carbonate-filled fracture simulation set shown in Figure 4. One pair of simulation sets has saturated hydraulic conductivity (K_{sat}) of the soil one order of magnitude greater and lesser than the base case, while the other similarly varies the carbonate K_{sat}. Less-permeable fracture fillings reduce MAI, in accord with intuition. The counter-intuitive decrease in MAI with increasing soil K_{sat} in Figure 5 is consistent with the findings of *Stothoff* [1997], who demonstrated that evaporation is more effective (limiting MAI) if K_{sat} increases without concurrent changes in the retention properties. If the retention properties change concurrently with K_{sat}, however, MAI increases with increasing soil K_{sat}.

The impact of the change in soil properties is fundamentally different from the impact of the fracture properties. A change in soil properties affects the slope of the response of MAI with soil thickness, while a change in filling properties only offsets the response curve. Changing the soil hydraulic properties affects the number and magnitude of wetting pulses reaching the soil/fracture interface; changing the fracture hydraulic properties only affects the rate at which wetting pulses enter the fracture and escape evaporation.

3.4 Climatic Variation

The response of MAI to various climatic factors, for two systems with 2 and 15 cm of soil over an unfilled fracture continuum, is shown in Figure 6. The same procedure was followed to produce Figure 2. The base-case unfilled-fracture and the base-case soil cover hydraulic properties in Table 1 are used. Fracture properties considered here are based on the range of parameters reported by

Schenker et al. [1995], and are representative of both the Tiva Canyon and the Topopah Springs densely welded tuffs. *Stothoff* [1997] found that the fracture properties do not materially impact simulated infiltration rates as long as there exists some small amount of unfilled fractures.

The response to each of the climatic factors is investigated by uniformly multiplying each of the hourly values in the decade by a scaling factor, except that MAT is investigated by adding a constant temperature to each of the hourly air temperatures. Note that climatic change will likely not occur in exactly this way, as there may be seasonality changes as well as magnitude changes, but the gross effect of climatic change may be captured through this approach. As with the deep-alluvium case, changes in precipitation and temperature have the largest impact on MAI, while shortwave radiation has minimal impact. Windspeed, vapor density, and longwave radiation have moderately small impacts.

Note that there is significantly increased sensitivity to climatic change as the soil thickness increases. For example, north-facing and south-facing slopes have essentially identical values of bare-soil MAI for the shallow soil while for the deeper soil north-facing slopes have about 2.5 times larger MAI than south-facing slopes. Clearly the depth of soil has a far more significant impact on MAI than most of the climatic inputs.

The response of MAI to MAP and MAT (the most significant meteorologic inputs identified in Figure 6), using the soil-over-carbonate system, is demonstrated in Figure 7. The base-case soil cover is used, and carbonate hydraulic properties are described by case cal3 in Table 1. In these simulations, MAI responds exponentially to MAP multiples and MAT changes. There is also an increased sensitivity to changes as the soil thickness increases. A similar behavior occurs for the set with soil over a soil-filled fracture.

3.5 Shallow Soil Over Bedrock Simulations

A few simulations were performed, for completeness, to investigate bare-soil MAI if no fractures are present. Simulations were performed with bedrock representative of densely welded tuffs (Tiva Canyon upper lithophysal, tcul; Topopah Spring lower nonlithophysal, tslnl), moderately welded tuffs (Tiva Canyon caprock, tccap), and nonwelded tuffs (Tiva Canyon shardy base, tcshar), with hydraulic properties reported in Table 1. Bedrock properties are based on values reported by *Flint et al.* [1996b], with samples TPC52s, PW19s, and BT26Hs used to provide retention properties. Two non to moderately welded tuffs (mw7, mw8) were also used with representative properties. Bare-soil MAI under nominal climatic conditions is shown in Figure 8.

Stothoff [1997] found that bare-soil MAI was negligible when the permeability of semi-infinite alluvium was less than 10^{-10} cm^2. If true of tuffs as well, only the semi-infinite tcshar tuffs might be permeable enough to exhibit significant bare-soil MAI. The densely welded tuffs (not shown) indeed exhibited little to no infiltration (< 0.001 mm/yr for tcul and < 1 mm/yr for tslnl) even with soil cover, but the more permeable tuffs exhibited significant infiltration. Of the tuffs with significant infiltration, only the caprock tuff is extensively exposed.

It is interesting to note that bare-soil MAI increases with increasing soil depth for very shallow soils over the less-permeable bedrock tuffs, in contrast to the case when unfilled fractures are considered. Significant MAI apparently requires extended contact time for moisture to enter the bedrock in these lower-permeability tuffs; without soil cover, precipitation simply runs off. It is expected that all of the non to moderately welded tuffs (with K_{sat} greater than the asymptotic deep-soil infiltration rate) will reach the asymptotic deep-soil rate shown in Figure 4 as soil depth increases. Densely welded tuffs with K_{sat} lower than the asymptotic rate should reach a deep-soil rate of approximately their K_{sat} value.

An additional simulation, labeled mw7d, is also shown in Figure 8. The mw7d simulation is identical to the corresponding mw7 simulation, except that the hourly meteorologic readings are used for case mw7 and daily meteorologic readings are used for case mw7d. Based on the difference between these simulations, it can be concluded that MAI may be significantly underestimated when daily readings are used. Other simulations (not shown) suggest that relative underestimation increases as MAI decreases. Most of the error arises from underpredicting depth of wetting-pulse penetration during and immediately after precipitation (thus over-predicting evaporation during this period), due to using the smaller daily flux rates. Further, atmospheric relative humidity tends to be higher on days with precipitation, lowering potential evaporation and allowing deeper penetration of wetting fronts. It is unlikely that using shorter boundary-condition periods (*e.g.*, 5 or 15 minutes) would affect evaporation significantly, but shorter periods may enhance runoff, thus lessening MAI.

Simulations using a mixture of hourly meteorologic inputs during the days in a period bracketing rainfall events, and monthly averaged inputs outside the bracketing period, suggest that a satisfactory bracket period should include the days before, during, and after precipitation. Because of the potential for misrepresentation of the processes, predictions generated using daily input should be viewed with caution.

4 RESPONSE FUNCTION ABSTRACTIONS

By performing a sufficient number of simulations of the flow of moisture and energy in a 1D column representative of the shallow surface of YM, changing hydraulic parameters and meteorologic inputs in a systematic way, it is possible to build up a response function describing the relationship between MAI and the input values. For a deep system, two major regions of response are identified depending on whether the soil permeability is above or below a critical value related to the typical storm intensity. For a two-layer system, the response also depends on whether the underlying system forms a capillary barrier or not.

Three types of response function abstractions for bare-soil MAI are presented in this section, all developed through trial and error. The first type is for semi-infinite soil (*i.e.*, greater than about 10 m in depth with underlying bedrock or bedrock fractures having sufficient permeability to accommodate the soil-derived fluxes). The second type is for shallow soil above a medium providing a neutral to strong capillary barrier (*e.g.*, soil-filled and unfilled fractures). The third type is for shallow soil above a permeable medium providing a neutral to strong capillary attractor (*e.g.*, soil- or carbonate-filled fractures and non to moderately welded tuffs). The second and third abstractions are almost identical in form, only differing by the representation of the dependence of MAI on soil thickness.

The three response function abstractions are primarily different in their treatment of soil thickness and the hydraulic properties of the underlying medium. The first abstraction does not consider soil thickness or the underlying medium. The second abstraction is strongly affected by soil thickness, but the properties of the underlying medium have little effect on estimated MAI. The third abstraction is moderately affected by soil thickness, and the properties of the underlying medium have a significant effect on estimated MAI. The first and second abstractions monotonically respond to changing inputs, while the third abstraction may feature a critical soil thickness that provides maximal MAI.

The third abstraction was developed with perturbations to only those inputs having large impacts on MAI, so that coefficients for unperturbed inputs cannot be determined. Undetermined coefficients are estimated by scaling the equivalent coefficients from the other abstractions.

To determine coefficients in the abstractions, an Excel 97 SR-1 spreadsheet was created with all simulation results and the corresonding abstraction predictions. The solver uses a generalized reduced gradient nonlinear optimization algorithm. The solver minimizes an objective function of the form

$$\left[\sum_{i}^{N} \frac{(Y_{si} - Y_{ai})^2}{N}\right]^{1/2}, \tag{1}$$

where Y_{si} and Y_{ai} are the log-10 simulation and abstraction predictions, respectively, and there are N predictions to match. The solver used a precision of 10^{-6}, tolerance of 10^{-3}, and convergence criterion of 10^{-4}, and was generally restarted once to polish the results. Several starting guesses were used, with the best results reported here.

4.1 Response Functions

The wide variation in MAI is most appropriately described in log space. Four general types of functions are used to describe the response of $\log_{10}$(MAI) to any particular input: (i) power-law function, $\mathcal{P}(x)$; (ii) logarithmic, $\mathcal{L}(x)$; (iii) limited logarithmic, $\mathcal{L}_1(x)$; and (iv) V-shaped logarithmic, $\mathcal{L}_2(x)$. Inputs that cause logarithmic change in $\log_{10}$(MAI) for one parameter range but little change for another range are described using the limited logarithmic function. Inputs that cause logarithmic change in $\log_{10}$(MAI) for two parameter ranges, but with different slopes, are described using the V-shaped logarithmic function. The V-shaped function is only used to describe the depth-dependence when capillary-attractor lower layers are used.

The four shape functions are defined by

$$\mathcal{P}(x) = \left(\frac{x}{x_0}\right)^a - 1 \tag{2}$$

$$\mathcal{L}(x) = \log_{10}\left(\frac{x}{x_0}\right) \tag{3}$$

$$\mathcal{L}_1(x) = \log_{10}\left[1 + \left(\frac{x}{x_0}\right)^a\right] \tag{4}$$

$$\mathcal{L}_2(x) = \log_{10}\left[1 + \left(\frac{x}{x_0}\right)^a + \left(\frac{x}{x_0}\right)^b\right] \tag{5}$$

where x is the variable of interest, x_0 is a normalizing value for the variable of interest, and a and b are constants with opposite sign.

After rearrangement and simplification, the relationship describing the response of bare-soil MAI to input parameters can be described generically as

$$H = \log_{10}\left(\frac{\text{MAI}}{\text{MAP}}\right) = A_1(S, F, W) + A_2(S, F, W)H, \tag{6}$$

where S, F, and W represent shape functions for soil (top layer), fracture (bottom layer), and weather inputs, respectively, and A_1 and A_2 represent combinations of these shape functions. The relationship can be rearranged as follows:

$$H = \frac{A_1}{1 - A_2}. \tag{7}$$

As a practical matter, certain combinations of inputs yield A_1 and A_2 such that H is incorrectly greater than 0. In such cases, if $A_2 < 1$ (generally for very wet and cool conditions), then H should be set to 0; otherwise, H should be set to some minimum cutoff value.

4.2 Deep Alluvium

The response of bare-soil MAI in deep alluvium is abstracted into two simple formulae accounting for soil properties and meteorologic inputs for two permeability ranges. One formula provides a servicable representation for bare-soil MAI in deep alluvial materials coarser than a loam or sandy loam texture. The other formula simply states that fine-textured media (*e.g.*, the fine extreme of soils and bare unfractured bedrock) have essentially zero MAI. The transition zone between these two ranges is not abstracted due to the complexity of the behavior, although the shallow-soil abstraction cases could be specialized to consider this case by imposing zero soil thickness in the abstraction.

Stothoff [1997] demonstrated that there are two distinct behaviors for MAI in deep alluvium, depending on the value for permeability. In low-permeability media ($k < 10^{-10}$ cm^2), MAI is essentially zero. In the low-permeability range, significant numbers of wetting events have rainfall rates too large for the ground to accept, runoff often occurs, and evaporation is able to reclaim the small amount of MAP that enters the ground. In high-permeability media ($k > 10^{-8}$ cm^2), there is a trend toward decreasing MAI with increasing permeability (holding other hydraulic properties constant). All precipitation is accepted into the ground; however, evaporation becomes more effective with increasing permeability, leaving less moisture for net infiltration.

The permeability range of 10^{-8} through 10^{-10} cm^2 is transitional from the behavior of high- to low-permeability media, and MAI appears to be strongly medium-dependent. The permeability yielding greatest MAI is in the transition zone between the two limiting permeability behavior zones; most events are accepted by the medium but some of the largest storms generate runoff. There is an extremely rapid dropoff in MAI as permeability decreases from the largest-MAI permeability; it appears that MAI may change several orders of magnitude with a change of less than one order of magnitude in permeability. No attempt is made to characterize the response of MAI in this zone; many further simulations would be necessary to provide a robust abstraction.

Characterizing the response of MAI to parameters of a low-permeability medium is quite straightforward. At the YM site, any imbibing water is removed by evaporation, so that MAI is zero, when soil or bare-bedrock permeability is below a cutoff permeability (approximately 10^{-9} to 10^{-10} cm^2). The formula for low-permeability media is simply

$$\text{MAI} \approx 0 \tag{8}$$

for permeability less than 10^{-10} cm^2. Based on this formula extrapolated from semi-infinite soil column simulations, no exposed unfractured bedrock at YM would be expected to have significant MAI.

High-permeability media provide quantifiable trends in the behavior of MAI, and this behavior is abstracted as

$$H = \log_{10}\left(\frac{\text{MAI}}{\text{MAP}}\right) = \alpha_0 + S(1 + \alpha_s H) + W(1 + \alpha_w H) \tag{9}$$

where the α parameters account for the increased sensitivity for smaller values of MAI. The relationship can be rearranged as follows:

$$A_1 = \alpha_0 + S + W \tag{10}$$

$$A_2 = \alpha_s S + \alpha_w W \tag{11}$$

$$S = s_1\mathcal{L}(k) + s_2\mathcal{P}(m) + s_3\mathcal{P}(P_c) + s_4\mathcal{P}(\varepsilon) \tag{12}$$

$$W = w_1\mathcal{L}(\text{MAP}) + w_2\mathcal{P}(\text{MAT}) + w_3\mathcal{P}(\text{MAV}) + w_4\mathcal{L}(\text{MAW}) + w_5\mathcal{L}(\text{MAR}) \tag{13}$$

where k is intrinsic permeability, m is van Genuchten $m = 1 - 1/n$, P_c is the reciprocal of van Genuchten α in pressure units, ε is porosity, and the remaining values are constants determined through least-squares minimization. Incoming radiation is calculated by summing longwave and net shortwave radiation (albedo is assumed to be 0.33).

The results from a total of 65 simulations of deep alluvium, all with permeability at least 10^{-8} cm^2, were used to determine the 12 fitting constants. All exponents were arrived at visually. The coefficients in the abstraction are presented in Table 2.

The only counter-intuitive behavior in the abstraction is for permeability, with decreasing MAI for increasing permeability. As discussed before, permeability is correlated to both van Genuchten m and P_c in such a way that MAI generally is larger for more permeable soils. Otherwise, MAI increases as precipitation increases and decreases as evaporation is enhanced.

4.3 Soil/Capillary-Barrier System

The soil/capillary-barrier system features a neutral to strong capillary barrier at the soil/fracture interface. The underlying medium is typically an unfilled fracture continuum, which requires saturation at the interface to initiate fracture flow. A soil-filled fracture represents a neutral endpoint for the abstraction. The abstraction is determined for bare-soil MAI when soil thicknesses are less than 50 cm, although as a practical matter can be used up to at least 5 m with the understanding that any MAI value below some cutoff (*e.g.*, 0.01 mm/yr) is essentially zero. Responses for soil thicknesses greater than 5 m begin to transition to the semi-infinite soil responses. As with the deep system, normalized MAI is used in the abstraction. Normalized MAI is dominated by soil moisture holding capacity above the soil/bedrock interface. There is a tendency for changing sensitivity as MAI decreases.

The relationship describing the response of bare-soil MAI to the input parameters is:

$$\begin{aligned} H = \log_{10}\left(\frac{\mathrm{MAI}}{\mathrm{MAP}}\right) &= \alpha_0 + F(1+\alpha_f H) \\ &\quad + [\alpha_1 + S(1+\alpha_s H) + W(1+\alpha_w H)]\mathcal{L}_1(B_b) + \alpha_{s2} S + \alpha_{w2} W \end{aligned} \tag{14}$$

The relationship can be rearranged as follows:

$$A_1 = \alpha_0 + F + (\alpha_1 + S + W)\mathcal{L}_1(B_b) + \alpha_{s2}S + \alpha_{w2}W \tag{15}$$

$$A_2 = \alpha_f F + (\alpha_s S + \alpha_w W)\mathcal{L}_1(B_b) \tag{16}$$

$$S = s_1\mathcal{L}_1(k_s) + s_2\left(\frac{m_s - m_{s0}}{m_{s0}}\right)^2 + s_3\mathcal{L}(P_{cs}) \tag{17}$$

$$F = f_1\mathcal{L}_1(k_f) + f_2\mathcal{P}(m_f) + f_3\mathcal{L}_1(P_{cf}) + f_4\mathcal{L}_1(\varepsilon_f) \tag{18}$$

$$W = w_1\mathcal{L}(\mathrm{MAP}) + w_2\mathcal{P}(\mathrm{MAT}) + w_3\mathcal{P}(\mathrm{MAV}) + w_4\mathcal{L}(\mathrm{MAW}) + w_5\mathcal{L}(\mathrm{MAR}) \tag{19}$$

where s and f subscripts represent soil and fracture, respectively, and B_b is the soil moisture holding capacity (pore space times soil thickness). The b subscript on B_b stands for a capillary barrier.

The constants in the response function determined by nonlinear least-square minimization are presented in Table 3. The mean of the squared deviates was 0.0145, using the results from 207 simulations that include simulations with unfilled and soil-filled fractures. Soil depths considered ranged from 2 cm through 50 cm. Additional simulations with MAI less than 0.02 mm/yr were considered inaccurate for estimation in log space and discarded.

Representative matches between simulation results and abstraction predictions are shown in Figure 9. Responses to changing soil and fracture hydraulic properties are shown in Figure 9a and b, respectively, while responses to changing meteorologic inputs are shown in Figure 9c. The response of MAI to the input parameters is captured adequately, with matches at worst within roughly a factor of two. The abstraction tends to have a flatter decrease in MAI with increasing soil thickness than do the simulation results. Note that the reliability of the simulation predictions decreases as the soil thickness increases, due to the dependence of MAI on the few wetting pulses large enough to initiate fracture flow. An improved fit to the unfilled-fracture results shown in Figure 9 can be achieved if the soil-filled-fracture simulations are not used; however, the range of parameters for which a robust abstraction is obtained is severely limited.

The response of MAI to the soil van Genuchten m parameter differs from the deep-soil case, in the sense that changing the parameter from the base case results in larger values of MAI regardless of whether the parameter is increased or decreased. The effect may be artificial. As MAI is quite insensitive to m, the functional representation capturing this effect has little effect on predictions for m in the range considered in simulations (0.1 to 0.3) but has a large effect outside the range. It is recommended that the soil van Genuchten m parameter not be used in abstractions, especially outside the range of 0.1 to 0.3.

4.4 Soil/Capillary-Attractor System

The soil/capillary-attractor system features a neutral to strong capillary attraction at the soil/fracture interface, in direct contrast to the soil/capillary-barrier system. In the case of capillary attraction, water is preferentially drawn into the fractures and retained against evaporation. Even though the permeability of unfilled fractures may be far larger than for filled fractures, the filled-fracture properties are more conducive to retaining imbibed water.

The only difference in the form of the abstraction between the two systems is how MAI responds to soil thickness. In the capillary-barrier system, B_b is only a function of soil moisture holding capacity, and $\log_{10}(\mathrm{MAI})$ monotonically changes with B_b. In the capillary-attractor system, however, the underlying medium may have sufficiently small permeability that a small amount of soil cover is required to promote infiltration. In this lower-permeability system, B_a (the subscript stands for attractor) is a function of soil moisture holding capacity, MAP, MAT, and the underlying permeability. There is also a tendency for increased sensitivity to inputs as MAI decreases.

The abstracted relationship describing the response of bare-soil MAI to the input parameters is:

$$H = \log_{10}\left(\frac{MAI}{MAP}\right) = \alpha_0 + F(1+\alpha_f H) + [\alpha_1 + S(1+\alpha_s H) + W(1+\alpha_w H)]\mathcal{L}_2(B_a) + \alpha_{s2}S + \alpha_{w2}W \tag{20}$$

The functional form of the shape function containing B_a allows increasing MAI with increasing soil thickness for shallow soils over low-permeability media. For a capillary attractor, B_a is defined by

$$B_a = \frac{\varepsilon_s b \exp(\mathrm{MAT}/\mathrm{MAT}_0) k_f}{\mathrm{MAP}}, \tag{21}$$

where ε_s is soil porosity and b is soil thickness. The other evaporation-affecting parameters may also modify B_a, to a lesser extent, but additional simulations would be required to investigate this hypothesis.

Constants with specified values were estimated by inspection. Only the response to MAP and MAT was directly investigated via simulation; the constants for the remaining meteorologic inputs were estimated by scaling the corresponding soil/capillary-barrier coefficients by the change in the MAT coefficients. The remaining constants in the response function were determined by nonlinear least-square minimization, and are presented in Table 4. The objective function was 0.0111, using the results from 142 simulations that include soil over carbonate-filled and soil-filled fractures as well as soil over bedrock (using the soil-filled-fracture simulations for both the capillary-attractor and capillary-barrier regressions). Soil depths considered ranged from 10 cm through 150 cm. Additional simulations with MAI less than 0.02 mm/yr were considered inaccurate for estimation in log space and discarded.

Representative matches between simulation results and abstraction predictions are shown in Figure 10. Responses to changing soil and fracture hydraulic properties are shown in Figures 10a and b, respectively, while responses to changing meteorologic inputs are shown in Figure 10c. The simulated and abstracted predictions shown in Figure 10 match considerably better than the capillary-barrier results; the better visual fit is corroborated by the smaller objective function. The better fit may be due to enhanced representativeness, since more wetting pulses will pass the soil/bedrock interface for any given soil thickness in capillary attractor systems than in capillary barrier systems. The lower value of soil saturation necessary to trigger fracture flow in capillary attractors means that smaller, more frequent pulses can reach the necessary threshold.

As with the soil/capillary-barrier abstraction, the soil van Genuchten m parameter should not be used in the abstraction, especially outside the range of 0.1 through 0.3.

5 ABSTRACTION PREDICTIONS

The bare-soil MAI abstractions developed in Section 4 can be used to make predictions for various combinations of climatic inputs and hydraulic properties. In particular, conditions that may arise in the future at YM are of particular interest. Elevation is used as a surrogate for climatic change, with several plausible soil and fracture combinations examined at each elevation. Elevations are selected to yield MAP of 1, 1.5, and 2 times estimated present-day MAP at YM. At each elevation, radiation loads for representative north-facing, south-facing, and horizontal surfaces are considered.

5.1 Meteorologic Inputs

Simple models are used here to estimate elevation-dependent distributions of meteorological factors. Presuming that long-wave radiation is essentially constant over YM and the sensitivity of MAI to long-wave radiation is relatively small, and noting that MAI is relatively insensitive to windspeed, these two factors are neglected in the current analysis. MAP is estimated by an exponential expression regressed by *Hevesi et al.* [1992], based on cokriged elevation and MAP for 42 stations in southwestern Nevada,

$$\text{MAP} = \exp(4.26 + 0.000646z) \tag{22}$$

where MAP is in cm/yr and z is ground-surface elevation in meters. The author is not aware of a similar regression for MAT or MAV, so the Desert Rock station (elevation about 1000 m) and a central Nevada meteorological station at elevation 2215 m [*McKinley and Oliver*, 1994] are used to estimate MAT and MAV, assuming temperature decreases linearly and vapor density decreases exponentially with elevation. The formulae used to estimate elevation-dependent distributions are:

$$\text{MAT} = 25.83 - 0.00840z \tag{23}$$

$$\text{MAV} = \exp(-11.96 - 0.000341z) \tag{24}$$

where MAT is in °C, and MAV is in gm/cm^3. A typical lapse rate for temperature is on the order of 5 to 6 °C/km [*Fairbridge*, 1967]; the somewhat higher rate of 8.4 °C/km used here may be attributed to the aridity of the southern Great Basin.

A 6 km E-W × 9 km N-S DEM of the subregional area, with a grid resolution of 30 m × 30 m, has a minimum elevation of 1110 m and maximum elevation of 1752 m, and elevation over the proposed repository footprint ranges from roughly 1250 to 1500 m. Over the DEM range in elevation, MAP ranges from 145 mm/yr to 220 mm/yr, MAT ranges from 11.1 °C to 16.5 °C, and MAV ranges from 3.17×10^{-6} gm/cm^3 to 2.59×10^{-6} gm/cm^3. Corresponding values from the Desert Rock data (elevation about 1000 m) are 163 mm/yr, 17.4 °C, and 4.52×10^{-6} gm/cm^3; the decade represented by the Desert Rock data is slightly wetter than predicted by the exponential expression (157 mm/yr).

Three elevations (1300, 1900, and 2400 m) are used to examine the impact of climatic change. These elevations correspond to 1, 1.5, and 2 times present-day MAP at YM, respectively. At these elevations, MAT is 2.5, 7.5, and 11.7 °C cooler than Desert Rock, while MAV is 0.91, 0.74, and 0.63 times the Desert Rock value.

The calculated value of MAI based on MAP, MAT, and MAV is modified by solar radiation, estimated by calculating the north-south and east-west rotations of the ground surface, and interpolating within a table of mean annual cloud-free shortwave radiation as a function of surface rotation. Annual shortwave radiation is uniformly scaled by a cloudiness factor to match the Desert Rock data; no attempt is made to adjust the factor for different elevations. Three sample angles are considered: upward-facing, 30 degrees south-facing, and 30 degrees north-facing, corresponding to a typical ridge at YM. For these angles, south-facing and north-facing slopes have MAR of 1.14 and 0.8 times the MAR for upward-facing locations. Shadowing, in which the sun is blocked by ridges for part of the day, may cause additional small impacts on MAI at YM.

Note that there can be interplay between cloudiness and precipitation affecting the MAI predicted by scaling cloud-free shortwave radiation that has a slight influence on the simulations, but is neglected here. In the Desert Rock data set, cloudiness tends to peak around 4 o'clock in the afternoon and has a minimum at about 2 o'clock in the morning, while average precipitation peaks about 3 o'clock in the afternoon. Both factors will tend to increase MAI for west-facing slopes relative to east-facing slopes, while not strongly affecting north- or south-facing slopes. The short-term timing of cloudiness and precipitation is more important as MAI increases, as the evaporation contact time is shorter. Conversely, as MAI decreases, MAI is more sensitive to variation in mean annual shortwave radiation.

5.2 Textural Inputs

Aside from alluvial deposits in wash bottoms and alluvial flats, the soil at YM today generally has a sandy loam texture due to Holocene æolian deposition. As discussed in Section 6.2, a much finer buried soil has been found in geologically stable locations, and similar finer soils have been found at higher elevations at an analog site.

The properties for three considered soils, using the soil survey in Table 2 by *Leij et al.* [1999], are presented in Table 5. These cases were selected to feature roughly an order of magnitude drop in K_{sat} from one case to the next, and should span the range of soils potentially present at YM. The sandy loam has a permeability roughly twice that estimated by *Schmidt* [1989] from texture, but is less than the estimate from several *in situ* tests using a bubbling permeameter (D. Or, personal communication, 1997). The abstracted response of the sandy loam is more questionable than the other soils, as the response is extrapolated from the simulations and sandy loam is in the high-to-low-permeability transition zone.

Three fracture scenarios are used for the example: (i) unfilled fractures, (ii) soil-filled fractures, and (iii) carbonate-filled fractures. The assumed hydraulic properties of the various media are reported in Table 5. The soil in soil-filled fractures is assumed to have the same properties as the overlying soil. The permeability and porosity values reported in Table 5 are multiplied by the fraction of bedrock area occupied by fractures (assumed to be 0.001 in all cases) when the medium occupies fractures, to account for the restriction in area available for flow.

5.3 Predictions

The predictions are laid out in Figure 11, with the columns corresponding to the overlying type of soil and the rows corresponding to the underlying type of fracture filling. For each soil/fracture case, nine climatic conditions are considered, corresponding to all combinations of three elevations and three solar aspects.

For all cases, bare-soil MAI decreases as the overlying soil becomes finer and increases as elevation increases. For the unfilled and soil-filled fracture cases (no capillary attraction to the underlying layer), MAI monotonically decreases with soil thickness, while with a capillary attraction there is a critical soil thickness causing maximal MAI.

Relative to uncertainties in hydraulic properties and alluvium depths, solar radiation has a relatively insignificant impact on MAI. Although direct solar-loading effects on MAI are not large, indirect effects may be significant, as vegetation and weathering rates (affecting soil texture) are also dependent on solar loading.

5.4 Impact of Spatial and Temporal Variability

Natural variability is unavoidable and ever-present. The meteorologic inputs used for the 1D simulations are relatively short in duration; over time, periods with similar duration may have MAP and MAT averages that vary considerably. The repository footprint at YM is roughly 5 km^2, while the horizontal scale of a 1D simulation might be several meters to several tens of meters, so that the horizontal scale of the simulations is 4 or 5 orders of magnitude smaller than the domain of interest. With this disparity in scales, spatial variability of hydraulic properties logically may play a significant role in the spatial average of MAI over the repository.

It is straightforward to evaluate the impact of natural variability using a Monte-Carlo analysis with the abstractions developed in Section 4. A Monte-Carlo analysis to determine the expected value of MAI is performed by generating numerous realizations of the input parameters, evaluating MAI for each realization using the abstraction, and averaging MAI over all realizations. A set of correlated normally (or lognormally) distributed input parameters is generated using the relationship

$$\frac{v_j - m_j}{s_j} = \chi_j, \tag{25}$$

$$\chi_j = \left[\frac{\rho_{ij}}{\left(\sum_{j=1}^{N} \rho_{ij} \right)^{1/2}} \right] \epsilon_i \tag{26}$$

where

j represents one of the N input parameters
v_j is the value of variable j
s_j is the standard deviation of variable j
m_j is the mean of variable j
χ_j is a vector of correlated perturbations with zero mean and unit variance
ρ_{ij} is the correlation between variables i and j
ϵ_i is a vector of independent normally distributed perturbations

The scaling of the correlation matrix ensures that the variance of the inputs is preserved.

The impact of natural variability on MAI can be examined using the same set of soil properties, fracture properties, and elevations used in Figure 11 (neglecting the impact of solar radiation). For convenience, it is assumed that all input properties are lognormally distributed except for MAT, which is normally distributed, and the mean and variance for all input properties are known. Uncertainty in the mean and variance description would have the effect of adding additional variability to the input parameter estimates.

Two assumptions regarding the mean values in Section 5.3 were examined: (i) the mean values are the most likely values, and (ii) the mean values are the arithmetic mean values. When the mean values were assumed to be arithmetic means, the log-mean values for lognormally distributed variables were adjusted by the following relationship [*Benjamin and Cornell*, 1970]

$$\ln m_Y = m_{\ln Y} + \frac{\sigma^2_{\ln Y}}{2}, \tag{27}$$

where Y is the lognormally distributed variable, $\ln m_Y$ is the logarithm of the mean of Y, $m_{\ln Y}$ is the mean of $\ln Y$, and $\sigma^2_{\ln Y}$ is the variance of $\ln Y$.

The standard deviation of decadal-average $\log_{10}(MAP)$ is assumed to be 0.1 and the standard deviation of decadal-average MAT is assumed to be 0.5 °C (based on daily readings from 1948 through 1993 at nearby Beatty, NV [*National Climatic Data Center*, 1994a]). Further, the correlation coefficient between the two averages is assumed to be 0.8.

For all soils, the standard deviation of $\log_{10}(K_{sat})$, $\log_{10}(P_c)$, $\log_{10}(\varepsilon)$, and $\log_{10}(b)$ are each assumed to be 0.3 (the high variability in ε is due to rock fragments). Further, it is assumed that K_{sat} and ε have a correlation coefficient of 0.65, K_{sat} and P_c have a correlation coefficient of -0.45, and P_c and ε have a correlation coefficient of -0.45, while variability in b is independent of the soil properties. The van Genuchten m parameter is not considered, as MAI is insensitive to it.

For all fracture continua, the standard deviation of $\log_{10}(K_{sat})$, $\log_{10}(P_c)$, $\log_{10}(\varepsilon)$, and $\log_{10}(m)$ are assumed to be 1, 1, 1, and 0.2, respectively. Further, it is assumed that K_{sat} and ε have a correlation coefficient of 0.25, K_{sat} and P_c have a correlation coefficient of -0.45, K_{sat} and m have a correlation coefficient of 0.25, P_c and ε have a correlation coefficient of -0.15, P_c and m have a correlation coefficient of -0.25, and m and ε have a correlation coefficient of 0.15. Correlations would probably be stronger for unfilled fractures, and soil and fracture-filling properties would likely be highly correlated in cases with soil-filled fractures, but these factors are not considered in the example.

To estimate the expected value of MAI using the Monte-Carlo approach, a vector of 10^5 correlated perturbations was generated for each input variable. Sufficient realizations are present so that, for computational efficiency, the same set of vectors was used for all combinations of soil, fracture, and soil thicknesses (only the mean values change). Reproducibility of results is excellent with this large number of realizations. The effect of natural variability is shown in Figure 12, which is based on the cases shown in Figure 11. For Figure 12, it is assumed that the values used in Figure 11 are the most-likely values. Only the lowest elevation is shown, for clarity; as elevation increases, the spread between perturbed and unperturbed predictions is reduced significantly.

The rapid dropoff of MAI with soil moisture holding capacity seen for some combinations of nominal conditions is reduced or eliminated when natural variability is accounted for. For unfilled fractures, by far the biggest influence on increased expected values of MAI is due to changing soil properties, in line with the insensitivity to fracture properties. On the other hand, variability in carbonate properties dominates the expected values of MAI for cases with carbonate-filled fractures. Interestingly, cases with soil-filled fractures see a small reduction in expected MAI for coarser-textured soils due to fracture-property variability. This reduction in expected MAI may be due to transitioning from capillary-attractor conditions to capillary-barrier conditions, and would not be expected if soil and fracture properties are highly correlated.

There is generally less than a factor of 3 or 4 increase in MAI due to climatic variability and the increase is largest for the low-MAI cases. High-MAI cases generally have impacts of 5 to 20 percent. Climatic-input variability has a relatively small impact on expected MAI, especially relative to variability in hydraulic properties. For the variability patterns in this example, the impact of MAT fluctuation on expected MAI is small (10 to 30 percent) of the impact due to MAP fluctuations.

Predictions using the assumption that the values used in Figure 11 are the arithmetic-mean values differ from those in Figure 12 in some filled-fracture cases, and incorporation of variability can reduce the expected values for MAI. The reduction is primarily due to the overall lower values for fracture properties, which act to systematically reduce MAI for some combinations of soil and filled-fracture properties. The dependence of MAI on soil thickness is greatly reduced when using the arithmetic-mean assumption.

Natural variability generally has the biggest effect on estimates when MAI is relatively small. Cases with coarser-textured soils are relatively unaffected by natural variability, in part due to the generally high values of MAI under nominal conditions. Even when there is little difference between the nominal and perturbed estimates, however, there may be considerable scatter in the individual perturbation realizations; the standard deviation of $\log_{10}$(MAI) is about 0.5 for the sandy loam simulations and between 1 and 1.5 for the finer-textured simulations.

If the statistical description used in the example is representative, different locations with the same nominal input properties may easily have MAI different by one to several orders of magnitude. In addition, in the majority of locations and most of the time, MAI will be less than the expected value of MAI. The important implication of this observation is that the bulk of infiltration would be expected to occur in local areas. Further, the bulk of MAI over long periods of time may occur during relatively infrequent large-magnitude excursions from the mean climatic conditions.

6 INFILTRATION DURING A GLACIAL CYCLE

Previous estimates of MAI at YM for the lifetime of the repository, required to calculate the percolation fluxes at and below the repository horizon that directly affect repository performance, have accounted for (at most) direct changes in MAI due to climate change, and generally do not account for short-term climatic variability during the cycle. Possible impacts of neglecting short-term variability are discussed in Section 6.1.

Every performance assessment to date has assumed that hydraulic properties and soil thicknesses remain constant over a glacial cycle. Field observations have been made that suggest that hydraulic properties have varied over glacial cycles, as is discussed in Section 6.2. During wetter portions of the glacial cycle, soil genesis processes are likely to have been enhanced, and it may be that YM soils were significantly deeper and finer-textured than at present. Periodically as conditions dried and warmed during the glacial cycle, a threshold dryness level may have been reached that resulted in vegetation replacement and drastically enhanced erosion over the repository footprint, resulting in soils that may have been shallower than those present now.

Because of the interplay of climate and soil-genesis/soil-erosion processes during a glacial cycle, the actual temporal pattern of MAI during the cycle is likely to have been significantly more complex than the climatic cycle itself. Accounting for changes in soil properties and depths is likely to dampen changes in MAI for much of the cycle, but may provide spikes of infiltrating water immediately subsequent to major erosional periods. Due to these dynamics, it is not clear that the assumptions of constant soil properties and thicknesses provide a bounding estimate of infiltration for performance assessment.

6.1 Direct Climatic Effects During a Glacial Cycle

Climate change at YM may not be merely a matter of the climate cycling between cooler/wetter and warmer/drier conditions. *Bull* [1991] discusses climate change over the past 25 ky in the southwestern United States, noting that available evidence suggests that four climates have characterized the region: full glacial, transitional, monsoonal, and interglacial (present-day). The full glacial climate was likely characterized by cooler conditions, increased winter precipitation, and decreased monsoonal precipitation relative to today, while the monsoonal likely had increased summer precipitation. Where vegetation at 1,200 m elevation in the Amargosa Desert is now dominated by desert thermophiles, succulents dominated during the monsoonal period and steppe shrubs dominated in full-glacial conditions [*Spaulding and Graumlich*, 1986]. The different climatic regimes are driven by insolation changes, which in turn affect glaciation, continental warming, and the position of the jet stream.

Changes in MAI due to climatic changes may be only coarsely approximated when using the abstractions developed herein. Seasonality changes are completely neglected, for example, as are the influences due to vegetation changes (as vegetation is neglected). On the other hand, predicting changes in seasonality over a future glacial cycle is fraught with uncertainty. It remains to be shown whether neglecting such influences has a large effect on estimates of MAI. For the purposes of performance assessment, it may be acceptable to neglect the details of climate change, particularly when several glacial cycles are considered, if reasonable upper-bound estimates of infiltration during climatic change are developed. As shown in Section 5.4, however, neglecting variability in climate on a relatively short-term scale will result in underestimates of infiltration.

The magnitude of the underestimation is assessed in this section for a representative glacial cycle using both a Monte-Carlo approach and a first-order approach. As an approximation to climate change for performance assessment, climatic factors are assumed to be described by a mean cycle with correlated first-order perturbations about the mean. These perturbations account for the variability missing by using the short timespan of meteorologic record. As the meteorologic record used in the simulations increases, the variance of the perturbations should decrease.

The mean signal for each climatic input is characterized by the form

$$U_i(t) = U_i(t_{PD}) + \eta_i(t)[U_i(t_{FGM}) - U_i(t_{PD})], \tag{28}$$

where U_i is the climatic input, t is time [T], t_{PD} and t_{FGM} represent present-day and full-glacial-maximum conditions, and $\eta_i(t)$ is the fraction of the full-glacial-maximum conditions (0 is present-day, 1 is full-glacial). For demonstration purposes,

$$\eta_i(t) = \eta(t) = \frac{\frac{1}{4}\left[1 - \sin[-\alpha(t + t_o)]\right]^2 - 0.06}{1 - 0.06}, \tag{29}$$

where $\alpha = 14.33$, $t_0 = 17.48$ ky, and t is in ky. The η curve is 0 at present and 1 at full glacial maximum, and yields conditions that are at least halfway to full glacial maximum for roughly two-thirds of the cycle. This representation for the mean glacial cycle is being used by the Nuclear Regulatory Commission (NRC) for performance assessment [*Mohanty and McCartin*, 1998].

It is assumed that there is no correlation between perturbations in successive time periods, although MAP and MAT are correlated within a time period. The method for generating perturbations discussed in Section 5.4 is also used to generate perturbations about the time-varying mean.

As shown in Section 5.4, the perturbations are fairly small for climatic variables, so that a first-order approach may be used to quantify the expected magnitude of the response of MAI to the input parameters. Perturbations due to hydraulic properties are large enough to render the first-order approximation questionable for these inputs.

If Y is a lognormally distributed random variable with mean m_Y, the mean value for Y is larger than the median value for Y ($\exp(m_{\ln Y})$, where $m_{\ln Y}$ is the mean of the logarithm of Y) if there is any variability in the process. The relationship between m_Y and $m_{\ln Y}$ is [*Benjamin and Cornell*, 1970]

$$\ln m_Y = m_{\ln Y} + \frac{\sigma^2_{\ln Y}}{2}, \tag{30}$$

where $\sigma^2_{\ln Y}$ is the variance of $\ln Y$.

The first-order approximation to the variance of random variable X, $\mathrm{Var}[X]$, can be expressed as a function of the variances of N random variables Y_i through the relationship [*Benjamin and Cornell*, 1970]

$$\mathrm{Var}[X] \approx \sum_{i=1}^{N}\sum_{j=1}^{N} \left.\frac{\mathrm{d}X}{\mathrm{d}Y_i}\right|_m \left.\frac{\mathrm{d}X}{\mathrm{d}Y_j}\right|_m \mathrm{Cov}[Y_i, Y_j] \tag{31}$$

where $\mathrm{Cov}[Y_i, Y_j]$ is the covariance between Y_i and Y_j. Thus, a first-order approximation to the expected value of MAI is

$$\ln(\mathrm{E}[X]) \approx \mathrm{E}[\ln X] + \frac{1}{2}\sum_{i=1}^{N}\sum_{j=1}^{N} \left.\frac{\mathrm{d}X}{\mathrm{d}Y_i}\right|_m \left.\frac{\mathrm{d}X}{\mathrm{d}Y_j}\right|_m \mathrm{Cov}[Y_i, Y_j] \tag{32}$$

where E[] is the expectation operator. In the approximation, X is log(MAI) and the Y inputs are log(MAP) and MAT. The derivatives are easily evaluated using finite differences.

A straightforward example demonstrates the effect of accounting for intermediate-scale perturbations over a glacial cycle. In Figure 13a, mean and perturbed values for MAP, MAT, and MAI are presented for one glacial cycle using a system of 30 cm of silty loam overlying a carbonate fracture system, with the same most-likely properties used in Section 5.4. For clarity, only one decade per century is plotted. Note that the MAI response is much greater than the relative perturbation to either MAP or MAT.

The ratio of MAI estimated using the perturbed climate to MAI estimated using glacial-mean climate is presented for the same soil types considered before (sandy loam, silt loam, and silty clay loam), each with 30 cm thickness overlying the same carbonate-filled fracture system (Figure 13b). The perturbed MAI is smoothed with a moving average of 300 entries for display clarity.

The first-order prediction is shown for each soil type. Under conditions where MAI is greater than a few percent of MAP, such as the sandy loam and the silt loam under glacial conditions, the first-order prediction is reasonably good. The first-order approach predicts that average bare-soil MAI over a glacial cycle is 68.4 mm/yr for sandy loam, while the Monte-Carlo approach predicts about 67.3 mm/yr and the unperturbed value is 61.8 mm/yr. Under low-MAI conditions (silty clay loam, silt loam under warm conditions) the first-order approach is rather poor, as would be expected from the large sensitivity to perturbations in these conditions. For silt loam, the average first-order, Monte-Carlo, and unperturbed values are 77, 8.6, and 5.4 mm/yr, respectively. The first-order method is unusable due to errors in drier conditions. Comparing Monte-Carlo and unperturbed results, there is a 1.6-fold increase in predicted MAI when climatic perturbations are considered. For silty clay loam, the first-order prediction is also unusable; the unperturbed value is 0.021 mm/yr while the Monte-Carlo approach predicts 0.57 mm/yr (a 27-fold increase when perturbations are considered). Note that horizontal segments of the first-order predictions occur where MAI is limited to 10^{-5} of MAP. The first-order approach should be practical for cases where nominal MAI is greater than a few percent of MAP, and appears to provide conservative estimates (*i.e.*, over-estimating MAI).

Based on Figure 13b, it can be seen that not accounting for climatic perturbation at YM yields MAI underestimates. If the soil maintains a sandy loam texture (which produces relatively large values of MAI) over the glacial cycle, underestimates will be relatively small (less than a factor of 1.5 at any point in the glacial cycle), not only for the example but for soil thicknesses of 10 and 50 cm (not shown). MAI in finer-textured soils may be underestimated by up to two orders of magnitude during parts of the cycle; however, the increase in MAI by one to two orders of magnitude may still yield an average MAI that is well less than 1 mm/yr for such soils.

It has not been demonstrated that using an expected climate smoothly varying through the period of repository performance will necessarily provide deep percolation fluxes at the repository horizon that are conservative or bound repository performance. Perturbations in conditions affecting MAI generate increased MAI, as demonstrated above. Similarly, occasional pulses in MAI due to perturbations in MAI over a glacial cycle may translate into increased releases from the repository. Conceivably, pulses in MAI may also result in pulses of higher radionuclide concentrations at receptor locations.

6.2 Textural Effects During a Glacial Cycle

Estimates of MAI at YM during climate change, necessary to calculate deep percolation fluxes and thereby assess performance of the repository over the lifetime of the radionuclide inventory, have typically assumed that hydraulic properties and soil depths remain constant over a glacial cycle. The assumption of constant soil depth is belied by the presence of remnant alluvial terraces in the YM washes. In Split Wash, for example, the channel has cut through alluvial terraces in the upper wash as much as 10 m to reach bedrock, removing 50 to 200 m^3/m of alluvium along the channel (unpublished data, S. Stothoff, 1998). Further, estimates of downgradient deposit volumes suggest that about 27 cm may have been removed from YM over the period of 11 to 2 ka [*TRW*, 1998], comparable to current cover thicknesses over the repository footprint.

NRC identified several sites in southern Nevada that are at higher elevations than YM and have tuffs overlain by shallow soil. These sites are potential analogs of YM under cooler and wetter conditions. The best analog site for the YM washes yet identified by the NRC is the east-draining Phinney Canyon watershed in the Grapevine Mountains, approximately 60 km west of YM. The NRC has identified a location at an elevation of about 2,150 m in Phinney Canyon where the densely welded tuff bedrock slopes are covered with a stable clay-loam soil approximately 50 cm deep. A layer of a similar soil has been found, buried by Holocene æolian deposits, immediately above bedrock in two erosionally stable locations at the edge of the caprock above Split Wash (personal communication, O. Chadwick, 1998). Clay loam thicknesses at the sites were 20 cm and 30 cm, respectively.

Analog sites are never perfect matches, of course, and the substitution of elevation for climate change is imperfect in part because the analog sites have also experienced climate change. Nevertheless, there is a tendency for higher-elevation analog sites to have a more-developed soil profile, both finer textured and thicker than presently exists at YM. As seen in Figure 11, the increase in MAI resulting from cooler and wetter climatic conditions may be completely counteracted if the soil texture is sufficiently finer, especially if the soil thickness increases. If YM experienced similar soils to those at the Phinney Canyon location, MAI would likely be much less than otherwise would be estimated when these soils were present. Even without accounting for transpiration, net infiltration may be significantly limited by changes in soil texture and depth.

Clay-rich soils require substantial periods of time to develop by weathering and dust input in arid climates, so that change in MAI due to increasing clay content may be gradual relative to climatic change. Soil development is promoted by moister conditions, warmer conditions, increased soil surface area, and the presence of vegetation to hold the soil in place. Soils may be relatively suddenly removed during climate change, however, if a threshold is passed where the vegetation mix changes and the replacements are less able to prevent erosion. There is evidence of at least six regional deposition events in nearby Crater Flat over the previous 730 ky [*Peterson et al.*, 1995], and numerous events in Fortymile Wash and Midway Valley [*TRW*, 1998], all suggestive of rapid stripping of accumulated soils held in hillslope storage.

Changing soil texture and thickness during a glacial cycle may have a profound effect on MAI, comparable to the direct effects due to MAP and MAT changes for portions of the cycle. These indirect soil-based effects tend to moderate the direct effects of climate change, by reducing MAI during cooler and wetter periods and increasing MAI during warmer and drier periods. Quantifying these indirect soil-based effects is more difficult than quantifying the direct effects, as soil genesis lags the onset of moister conditions and soil removal may respond quickly to drier conditions when a threshold level is reached.

7 CONCLUSIONS

The spatial distribution of mean annual infiltration below the active evapotranspiration zone is of great interest for evaluating the performance of the proposed high-level waste repository at YM. In order to address the issue, numerical studies examining the sensitivity of MAI to various hydraulic and meteorologic parameters were undertaken. *Stothoff* [1997] examined the influence of hydraulic parameters on MAI, finding that for a 1D bare-soil system with colluvium overlying an unfilled-fracture continuum, depth of colluvium is a dominant influence on MAI. The hydraulic properties of colluvium are also significant in estimating MAI. The underlying unfilled-fracture properties were found not to affect MAI significantly, as long as the fracture density is great enough to accept water pulses. As the magnitude of variability in MAI that might occur due to variability and uncertainty in hydraulic properties is much larger than the magnitude of variability in MAI that might occur solely due to the elevational distribution of meteorologic inputs, it can be concluded that properly characterizing hydraulic properties is more important for estimating the spatial distribution of MAI. In particular, the nature of the underlying bedrock fractures and fillings (*e.g.*, unfilled, carbonate-filled, or soil-filled) is critical to estimating MAI.

Using around 400 simulations, including those presented by *Stothoff* [1997], abstractions were developed herein to quantify the effect of hydraulic properties and mean annual meteorologic inputs on bare-soil MAI for deep alluvium, shallow-soil/fracture systems, and shallow-soil/bedrock systems. When soils are extremely shallow, unfilled fractures may provide the largest values of MAI due to favorable fracture permeability; however, as soil thicknesses increase beyond roughly 10 cm, filled fractures may provide larger values of MAI due to favorable retention properties. In general, the bedrock cropping out over the repository is too impermeable to support significant infiltration under current conditions, although some of the non to moderately welded tuffs may exhibit infiltration with a layer of soil covering the bedrock. Under wetter and cooler conditions and with a fine-textured soil cover, however, bedrock may provide the dominant pathway for infiltration. It was found that, in general, the sensitivity of MAI to meteorologic influences increases as MAI decreases.

Through examination of representative cases, soil and fracture hydraulic properties were found to have a more profound effect on MAI than meteorologic inputs. When the underlying medium is a capillary barrier (*e.g.*, an unfilled-fracture continuum), MAI was more sensitive to the soil properties, while the opposite is often the case for capillary attractors. Thickness of soil cover may have the most consistently important impact on MAI among all of the individual hydraulic parameters. Of the meteorologic inputs, MAP and MAT have the greatest effect on MAI, but at the YM scale the spatial distribution of these factors is not large enough to have a great impact on MAI relative to variation in MAI due to potential variability in hydraulic properties. When MAP and MAT are changed due to climate change, however, the impact on MAI is much larger.

Accounting for natural variability of input parameters generally results in increased expected values of MAI. Increases in expected MAI of several orders of magnitude can be seen for deep fine-textured soils when plausible hydraulic-property variability is imposed. For cases with high MAI under most-likely conditions, the increase in expected MAI may be quite small (even though individual realizations may vary by one or more orders of magnitude). Relatively short-term climate perturbations about the mean climatic signal also resulted in an increase of MAI relative to the MAI resulting from the most-likely climatic signal, due to the exponential response of bare-soil MAI to climate change. In the examples examined, the increase ranged between 10 and 400 percent. If the exponential response of bare-soil MAI to climate change is also seen when transpiration is accounted for, relatively small changes in climate may produce significant changes in paleoclimatic proxy records.

Indirect influences from climate change may also provide a potentially significant impact on MAI at YM; under cooler and wetter conditions, soil-genesis processes may result in finer soils that limit infiltration. However, slow-developing finer soils may be quickly stripped as warmer and drier conditions pass through a threshold level where the vegetation mix changes. Work is currently underway toward estimating the effect of soil genesis on MAI at YM.

Although the meteorological record is too short to provide truly representative long-term infiltration behavior for this semiarid site, significant insight on expected infiltration behavior is gained for a range of conditions expected over a glacial cycle. There are obvious limitations in the approach, as lateral redistribution, stratification, fast pathways, vegetation, and matrix-fracture interactions are not considered. It is expected that neglecting vegetation, in particular, introduces a consistent bias toward overestimating MAI, so that the estimates presented here are likely upper-bound estimates. Nevertheless, the approaches presented here provide considerable insight into the impact of hydraulic properties and climatic change on expected MAI over extended periods of time.

This paper was prepared to document work performed by the Center for Nuclear Waste Regulatory Analyses (CNWRA) for the NRC under Contract No. NRC-02-97-009. The activities reported here were performed on behalf of the NRC Office of Nuclear Material Safety and Safeguards, Division of Waste Management. The paper is an independent product of the CNWRA and does not necessarily reflect the views or regulatory position of the NRC. The BREATH code used in this paper is configured under the CNWRA's Software Configuration Procedure. The author would like to acknowledge the suggestions and comments made by R. Fedors, D. Or, O. Chadwick, D. Woolhiser, and B. Sagar, which tremendously improved the quality of this paper.

8 REFERENCES

Baumhardt, R. L. and R. J. Lascano. 1993. Physical and hydraulic properties of a calcic horizon. *Soil Science 155*(6), 368–375.

Benjamin, J. R. and C. A. Cornell. 1970. *Probability, Statistics, and Decision for Civil Engineers.* New York, NY: McGraw-Hill.

Bodvarsson, G. and T. M. Bandurraga (Eds.). 1996. *Development and Calibration of the Three-Dimensional Site-Scale Unsaturated Zone Model of Yucca Mountain, Nevada*, LBNL-39315, Berkeley, CA. Lawrence Berkeley Laboratory.

Bodvarsson, G. S., T. M. Bandurraga, and Y. S. Wu (Eds.). 1997. *The Site-Scale Unsaturated Zone Model of Yucca Mountain, Nevada, for the Viability Assessment*, LBNL-40376, Berkeley, CA. Lawrence Berkeley Laboratory.

Bull, W. B. 1991. *Geomorphic Responses to Climatic Change.* Oxford, England: Oxford University Press.

Coleman, N., N. Eisenberg, N. Stablein, D. Brooks, R. Fedors, B. Sagar, and S. Stothoff. 1998. NRC Issue Resolution Status Report on Yucca Mountain Present-day Shallow Groundwater Infiltration. *Supplement to Eos, Transactions 79*(45), F309.

Czarnecki, J. B. 1985. *Simulated Effects of Increased Recharge on the Ground-Water Flow System of Yucca Mountain and Vicinity, Nevada-California.* Water-Resources Investigations Report 84-4344, United States Geological Survey, Denver, CO.

Day, W. C., C. J. Potter, D. S. Sweetkind, and C. A. S. Juan. 1998. *Bedrock geologic map of the central block area, Yucca Mountain, Nye County, Nevada.* Miscellaneous Investigations Series I-2601, United States Geological Survey, Denver, CO.

Electric Power Research Institute. 1990. *Demonstration of a Risk-Based Approach to High-Level Waste Repository Evaluation.* EPRI NP-7057, Electric Power Research Institute, Palo Alto, CA.

Electric Power Research Institute. 1992. *Demonstration of a Risk-Based Approach to High-Level Waste Repository Evaluation: Phase 2.* EPRI TR-100384, Electric Power Research Institute, Palo Alto, CA.

Electric Power Research Institute. 1996. *Yucca Mountain Total System Performance Assessment, Phase 3.* EPRI TR-107191, Electric Power Research Institute, Palo Alto, CA.

Fairbridge, R. W. (Ed.). 1967. *The Encyclopedia of Atmospheric Sciences and Astrogeology.* New York, NY: Reinhold Publishing Corporation.

Flint, A. L. and L. E. Flint. 1994. Spatial Distribution of Potential Near Surface Moisture Flux at Yucca Mountain. In *Proceedings of the Fifth Annual International Conference on High Level Radioactive Waste Management*, La Grange Park, IL, pp. 2352–2358. American Nuclear Society.

Flint, A. L., L. E. Flint, and J. A. Hevesi. 1993. The Influence of Long Term Climate Change on Net Infiltration at Yucca Mountain. In *Proceedings of the Fourth Annual International Conference on High Level Radioactive Waste Management*, La Grange Park, IL, pp. 152–159. American Nuclear Society.

26/45

Flint, A. L., J. A. Hevesi, and L. E. Flint. 1996a. *Conceptual and Numerical Model of Infiltration for the Yucca Mountain Area, Nevada.* Milestone 3GUI623M, Department of Energy, Las Vegas, NV.

Flint, L. E., A. L. Flint, and J. A. Hevesi. 1994. Shallow Infiltration Processes in Arid Watersheds at Yucca Mountain, Nevada. In *Proceedings of the Fifth Annual International Conference on High Level Radioactive Waste Management,* La Grange Park, IL, pp. 2315–2322. American Nuclear Society.

Flint, L. E., A. L. Flint, T. C. Moyer, and J. K. Geslin. 1995. Lateral Diversion of Water in the Paintbrush Tuff Nonwelded Hydrologic Unit, Yucca Mountain, Nevada. *Supplement to Eos, Transactions 76*(46), F182.

Flint, L. E., A. L. Flint, C. A. Rautman, and J. D. Istok. 1996b. *Physical and Hydrologic Properties of Rock Outcrop Samples at Yucca Mountain, Nevada.* Open-File Report 95-280, United States Geological Survey, Denver, CO.

Hennessy, J. T., R. P. Gibbens, J. M. Tromble, and M. Cardenas. 1983. Water properties of caliche. *Journal of Range Management 36*(6), 723–726.

Hevesi, J. A. and A. L. Flint. 1993. The Influence of Seasonal Climatic Variability on Shallow Infiltration at Yucca Mountain. In *Proceedings of the Fourth Annual International Conference on High Level Radioactive Waste Management,* La Grange Park, IL, pp. 122–131. American Nuclear Society.

Hevesi, J. A., A. L. Flint, and L. E. Flint. 1994. Verification of a 1-Dimensional Model for Predicting Shallow Infiltration at Yucca Mountain. In *Proceedings of the Fifth Annual International Conference on High Level Radioactive Waste Management,* La Grange Park, IL, pp. 2323–2332. American Nuclear Society.

Hevesi, J. A., J. D. Istok, and A. L. Flint. 1992. Precipitation Estimation in Mountainous Terrain Using Multivariate Geostatistics. Part I: Structural Analysis. *Journal of Applied Meteorology 31*(7), 661–676.

Hudson, D. B., A. L. Flint, and W. R. Guertal. 1994. Modeling a Ponded Infiltration Experiment at Yucca Mountain, NV. In *Proceedings of the Fifth Annual International Conference on High Level Radioactive Waste Management,* La Grange Park, IL, pp. 2168–2174. American Nuclear Society.

Kwicklis, E. M., A. L. Flint, and R. W. Healy. 1994. Simulation of Flow in the Unsaturated Zone Beneath Pagany Wash, Yucca Mountain. In *Proceedings of the Fifth Annual International Conference on High Level Radioactive Waste Management,* La Grange Park, IL, pp. 2341–2351. American Nuclear Society.

Leij, F. J., W. J. Alves, M. T. van Genuchten, and J. R. Williams. 1999. The UNSODA Unsaturated Soil Hydraulic Database. In *Workshop on the Characterization and Measurement of the Hydraulic Properties of Unsaturated Porous Media,* Riverside, CA. University of California. In press.

Long, A. and S. W. Childs. 1993. Rainfall and Net Infiltration Probabilities for Future Climate Conditions at Yucca Mountain. In *Proceedings of the Fourth Annual International Conference on High Level Radioactive Waste Management,* La Grange Park, IL, pp. 112–121. American Nuclear Society.

McKinley, P. and T. Oliver. 1994. *Meteorological, Stream-Discharge, and Water-Quality Data for 1986 through 1991 from Two Small Basins in Central Nevada.* Open-File Report 93-651, United States Geological Survey, Denver, CO.

Mohanty, S. and T. J. McCartin. 1998. *Total-System Performance Assessment (TPA) Version 3.2 Code: Module Descriptions and User's Guide.* , Center for Nuclear Waste Regulatory Analyses, San Antonio, TX.

Montazer, P. and W. E. Wilson. 1984. *Conceptual Hydrologic Model of Flow in the Unsaturated Zone, Yucca Mountain, Nevada.* Open-File Report 84-4345, United States Geological Survey, Lakewood, CO.

National Climatic Data Center. 1994a. *WBAN Daily Surface Observations (1948 to 1994).* Asheville, NC: National Oceanic and Atmospheric Administration.

National Climatic Data Center. 1994b. *WBAN Hourly Surface Observations (1984 to 1994).* Asheville, NC: National Oceanic and Atmospheric Administration.

Nuclear Regulatory Commission. 1992. *Initial Demonstration of the NRC's Capability to Conduct a Performance Assessment for a High-Level Waste Repository.* NUREG-1327, Nuclear Regulatory Commission, Washington, DC.

Nuclear Regulatory Commission. 1995. *NRC Iterative Performance Assessment Phase 2: Development of Capabilities for Review of a Performance Assessment for a High-Level Waste Repository.* NUREG-1464, Nuclear Regulatory Commission, Washington, DC.

Peterson, F. F., J. W. Bell, R. I. Dorn, A. R. Ramelli, and T. L. Ku. 1995. Late Quaternary Geomorphology and Soils in Crater Flat, Yucca Mountain, Southern Nevada. *Geological Society of America - Bulletin 107*(4), 379–395.

Sandia National Laboratories. 1992. *TSPA 1991: An Initial Total-System Performance Assessment for Yucca Mountain.* SAND91-2795, Sandia National Laboratories, Albuquerque, NM.

Sandia National Laboratories. 1994. *Total-System Performance Assessment for Yucca Mountain–SNL Second Iteration (TSPA-1993).* SAND93-2675, Sandia National Laboratories, Albuquerque, NM.

Schenker, A. R., D. C. Guerin, T. H. Robey, C. A. Rautman, and R. W. Barnard. 1995. *Stochastic Hydrogeologic Units and Hydrogeologic Properties Development for Total-System Performance Assessments.* SAND94-0244, Sandia National Laboratories, Albuquerque, NM.

Schmidt, M. R. 1989. Classification of Upland Soils by Geomorphic and Physical Properties Affecting Infiltration at Yucca Mountain, Nevada. Master's thesis, Colorado School of Mines, Golden, CO.

Spaulding, W. G. and L. J. Graumlich. 1986. The last pluvial climatic episodes in the deserts of southwestern North America. *Nature 320*, 441–444.

Stothoff, S., D. Or, and D. Groeneveld. 1997. Hydrologic Interactions in Shallow Vegetated Soil Overlying Fissured Bedrock. *Supplement to Eos, Transactions 78*(46), F262.

Stothoff, S. and B. Sagar. 1997. Estimating Spatial and Temporal Variations of Infiltration at Waste Sites. In *Transactions of the American Nuclear Society*, Volume 76, La Grange Park, IL, pp. 203–205. American Nuclear Society.

Stothoff, S. A. 1995. *BREATH Version 1.1-Coupled Flow and Energy Transport in Porous Media: Simulator Description and User Guide.* NUREG/CR 6333, Nuclear Regulatory Commission, Washington, DC.

Stothoff, S. A. 1997. Sensitivity of long-term bare soil infiltration simulations to hydraulic properties in an arid environment. *Water Resources Research 33*(4), 547–558.

Stothoff, S. A., H. M. Castellaw, and A. C. Bagtzoglou. 1995. Estimation of Spatial Distribution of Recharge Factors at Yucca Mountain. In B. Sagar (Ed.), *NRC High-Level Radioactive Waste Research at CNWRA, January-June 1995*, Volume CNWRA 95-01S, San Antonio, TX, pp. 9-5–9-12. Center for Nuclear Waste Regulatory Analyses.

Stothoff, S. A., H. M. Castellaw, and A. C. Bagtzoglou. 1996. *Simulating the Spatial Distribution of Infiltration at Yucca Mountain, Nevada.* , Center for Nuclear Waste Regulatory Analyses, San Antonio, TX.

Sweetkind, D. S., E. R. Verbeek, J. K. Geslin, and T. C. Moyer. 1996. *Fracture Character of the Paintbrush Tuff Nonwelded Hydrologic Unit, Yucca Mountain, Nevada.* Administrative Report, United States Geological Survey, Denver, CO.

TRW. 1995. *Total System Performance Assessment-1995: An Evaluation of the Potential Yucca Mountain Repository.* B00000000-01717-2200-00136, TRW Environmental Safety Systems Inc., Las Vegas, NV.

TRW. 1998. *Yucca Mountain Site Description.* B00000000-01717-5700-00019 REV 00, TRW Environmental Safety Systems Inc., Las Vegas, NV.

Winterle, J. R., R. W. Fedors, D. L. Hughson, and S. Stothoff. 1999. *Review of the Unsaturated Zone Models to Support the Viability Assessment of a Repository at Yucca Mountain.* Letter Report, Center for Nuclear Waste Regulatory Analyses, San Antonio, TX.

Woolhiser, D. A., S. Stothoff, and G. W. Wittmeyer. 1997. Estimating Recharge Through the Ephemeral Channels of Solitario Canyon–Yucca Mountain, Nevada. *Supplement to Eos, Transactions 78*(46), F262–F263.

Woolhiser, D. A., S. A. Stothoff, and G. W. Wittmeyer. 1999. Estimating Channel Infiltration From Surface Runoff in the Solitario Canyon Watershed, Yucca Mountain, Nevada. *Journal of Hydrologic Engineering, American Society of Civil Engineers.* In review.

Table 1: Hydraulic properties used to assess infiltration sensitivity. Note that only one property is perturbed for each simulation.

Case	Intrinsic Permeability (cm^2)	Saturated Hydraulic Conductivity (mm/yr)	van Genuchten m	Bubbling Pressure (kPa)	Porosity
Soil cover					
Low perturbation	10^{-9}	3.1×10^{4}	0.1	1	0.2
Base case	10^{-8}	3.1×10^{5}	0.2	2	0.3
High perturbation	10^{-7}	3.1×10^{6}	0.3	5	0.5
Unfilled fracture					
Low perturbation	1.15×10^{-4}	3.6×10^{9}	0.6	9.8×10^{-4}	10^{-4}
Base case	1.15×10^{-2}	3.6×10^{11}	0.7	9.8×10^{-3}	10^{-3}
High perturbation	1.15	3.6×10^{13}	0.8	9.8×10^{-2}	10^{-2}
Carbonate-filled fracture					
Low perturbation	1.15×10^{-11}	3.6×10^{2}	0.4	–	10^{-5}
Base case	1.15×10^{-10}	3.6×10^{3}	0.5	10	10^{-4}
High perturbation	1.15×10^{-9}	3.6×10^{4}	0.6	100	–
cal3	5.7×10^{-10}	1.8×10^{4}	0.5	10	10^{-4}
Soil-filled fracture					
Low perturbation	–	–	–	–	10^{-4}
Base case	10^{-8}	3.1×10^{5}	0.2	2	10^{-3}
High perturbation	–	–	–	–	10^{-2}
Bedrock					
tcshar	1.6×10^{-9}	4.9×10^{4}	0.237	330	0.235
tccap	3.2×10^{-12}	99	0.301	200	0.105
tcul	9.1×10^{-15}	0.28	0.310	340	0.108
tslnl	1.7×10^{-13}	5.3	0.236	315	0.141
mw7	1.15×10^{-10}	3.6×10^{3}	0.480	120	0.283
mw8	1.15×10^{-11}	3.6×10^{2}	0.435	150	0.226

Table 2: Coefficients for deep-alluvium bare-soil MAI response to hydraulic and meteorologic inputs. The objective function is 0.0162 using 65 values. Exponents are all estimated visually.

Parameter	Function	Reference Value	Coefficient	Exponent
α_0	–	–	-1.3509	–
α_s	–	–	0.0370	–
α_w	–	–	-1.3000	–
Soil properties				
k (cm^2)	$\mathcal{L}$	10^{-8}	-0.5835	–
m	$\mathcal{P}$	0.2	0.6730	2
P_c (kPa)	$\mathcal{P}$	2	1.6127	-0.5
ε	$\mathcal{P}$	0.3	-1.0126	1
Meteorologic inputs				
MAP (mm/yr)	$\mathcal{L}$	162.8	0.8389	–
MAT (K)	$\mathcal{P}$	290.31	-4.9504	1
MAV (gm/cm^3)	$\mathcal{P}$	4.842×10^{-6}	0.1122	2
MAR (W/m^2)	$\mathcal{L}$	483.3	-0.4570	–
MAW (m/s)	$\mathcal{L}$	4.18	-0.1261	–

Table 3: Coefficients for bare-soil MAI response to hydraulic and meteorologic inputs for soil over a unfilled- or soil-filled fracture continuum. The objective function is 0.0145 using 207 values.

Parameter	Function	Reference Value	Coefficient	Exponent
α_0	–	–	0.0611	–
α_1	–	–	-0.0415	–
α_s	–	–	-0.4049	–
α_f	–	–	-4.5757	–
α_w	–	–	-0.1769	–
α_{s2}	–	–	2.5714	–
α_{w2}	–	–	-2.2809	–
B	$\mathcal{L}_1$	1.0053	–	3.9509
Soil properties				
k (cm^2)	$\mathcal{L}_1$	4.951×10^{-11}	-0.8940	0.0705
m	$[(m-m_0)/m_0]^2$	0.2030	1.1438[b]	2[a]
P_c (kPa)	$\mathcal{L}_1$	2[a]	-0.9476	–
Fracture properties				
k (cm^2)	$\mathcal{L}_1$	2.718×10^{-9}	4.3370	-2.2429
m	$\mathcal{P}$	0.4[a]	0.1437	-0.2143
P_c (kPa)	$\mathcal{L}$	1[a]	0.0096	–
ε	$\mathcal{L}_1$	0.1884	-0.4054	-0.0205
Meteorologic inputs				
MAP (mm/yr)	$\mathcal{L}$	162.8[a]	0.3367	–
MAT (K)	$\mathcal{P}$	290.31[a]	-2.9743	1[a]
MAV (gm/cm^3)	$\mathcal{P}$	4.84×10^{-6}[a]	0.0608	2[a]
MAR (W/m^2)	$\mathcal{L}$	483.3[a]	-0.0609	–
MAW (m/s)	$\mathcal{L}$	4.18[a]	-0.1581	–
[a] Imposed by inspection				
[b] Use 0 for m outside the range 0.1 through 0.3				

Table 4: Coefficients for bare-soil MAI response to hydraulic and meteorologic inputs for soil over a carbonate- or soil-filled fracture continuum or over unfractured bedrock. The objective function is 0.0111 using 142 values.

Parameter	Function	Reference Value	Coefficient	Exponent
α_0	–	–	14.629	–
α_l	–	–	-46.856	–
α_s	–	–	-70.430	–
α_f	–	–	-2.5189	–
α_w	–	–	-16.223	–
α_{s2}	–	–	28.729	–
α_{w2}	–	–	7.8008	–
B	$\mathcal{L}_2$	2.781×10^{-10}	–	0.2449,-0.1668
Soil properties				
k (cm^2)	$\mathcal{L}_1$	2.151×10^{-9}	-0.0442	0.0705
m	$[(m-m_0)/m_0]^2$	0.1993	0.2295[b]	2[a]
P_c (kPa)	$\mathcal{L}_1$	2[a]	-0.7028	–
Fracture properties				
k (cm^2)	$\mathcal{L}_1$	3.768×10^{-11}	0.0734	37.422
m	$\mathcal{P}$	0.4[a]	-0.1574	-2.8800
P_c (kPa)	$\mathcal{L}$	1[a]	0.6056	–
ε	$\mathcal{L}_1$	0.0292	0.0184	45.851
Meteorologic inputs				
MAP (mm/yr)	$\mathcal{L}$	162.8[a]	3.8634	–
MAT (K)	$\mathcal{P}$	290.31[a]	-41.348	1[a]
MAV (gm/cm^3)	$\mathcal{P}$	4.84×10^{-6}[a]	0.7717[c]	2[a]
MAR (W/m^2)	$\mathcal{L}$	483.3[a]	-0.7729[c]	–
MAW (m/s)	$\mathcal{L}$	4.18[a]	-2.0061[c]	–

[a] Imposed by inspection
[b] Use 0 for m outside the range 0.1 through 0.3
[c] Estimated by scaling the corresponding unfilled-fracture coefficients

Table 5: Hydraulic properties used to demonstrate the impact of texture on MAI.

Case	Intrinsic Permeability (cm^2)	Saturated Hydraulic Conductivity (mm/yr)	van Genuchten m	Bubbling Pressure (kPa)	Porosity
Sandy loam	1.3×10^{-8}	3.9×10^{5}	0.47	1.3	0.41
Silt loam	1.3×10^{-9}	3.9×10^{4}	0.29	4.9	0.45
Silty clay loam	2.0×10^{-10}	6.1×10^{3}	0.19	9.8	0.43
Unfilled fracture	1.15×10^{-2}	3.6×10^{11}	0.7	9.8×10^{-3}	1.00
Carbonate filling	1.15×10^{-11}	3.6×10^{3}	0.5	10	0.50

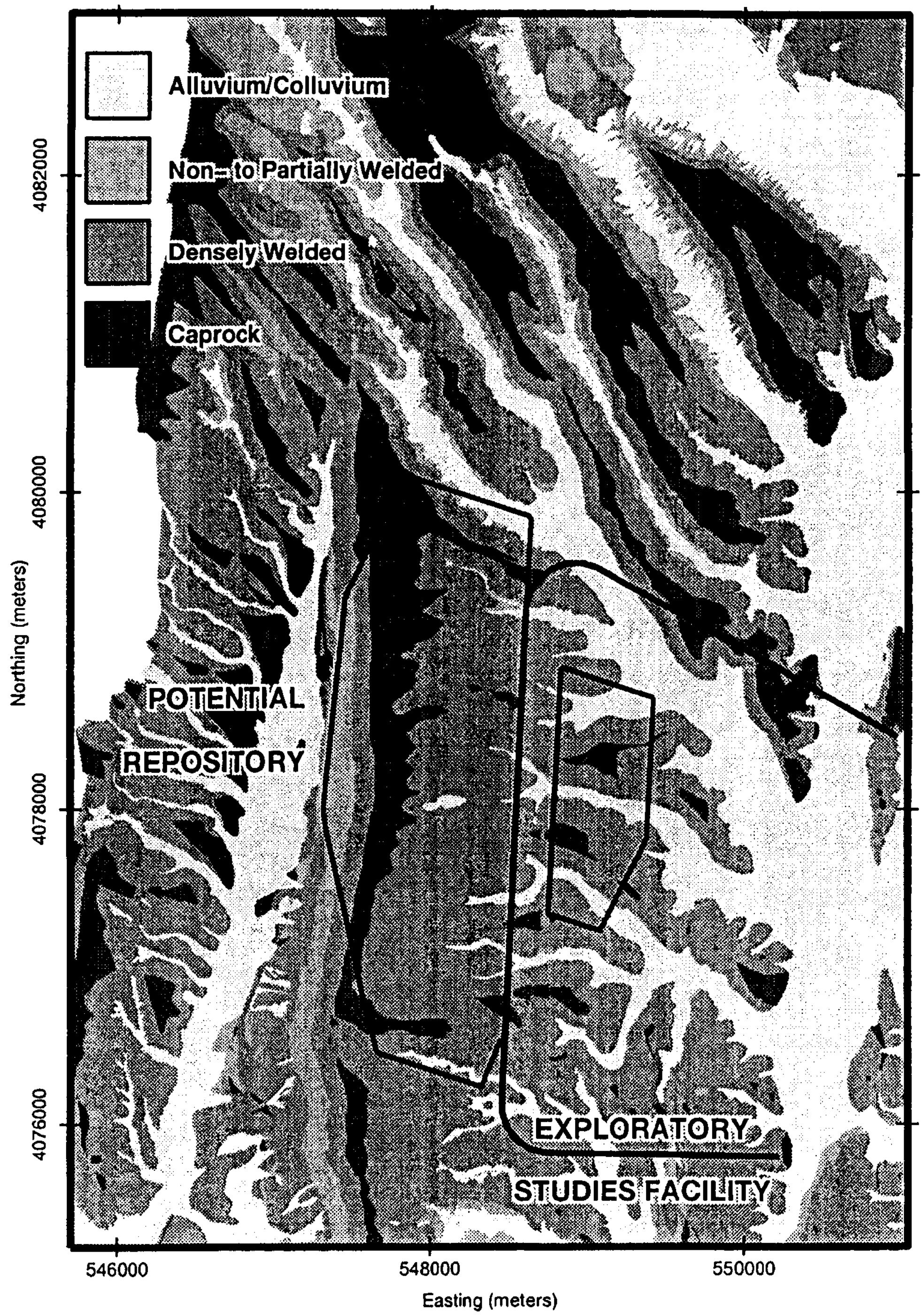

Figure 1: Geologic outcrops and proposed repository footprint (map based on *Day et al.* [1998]).

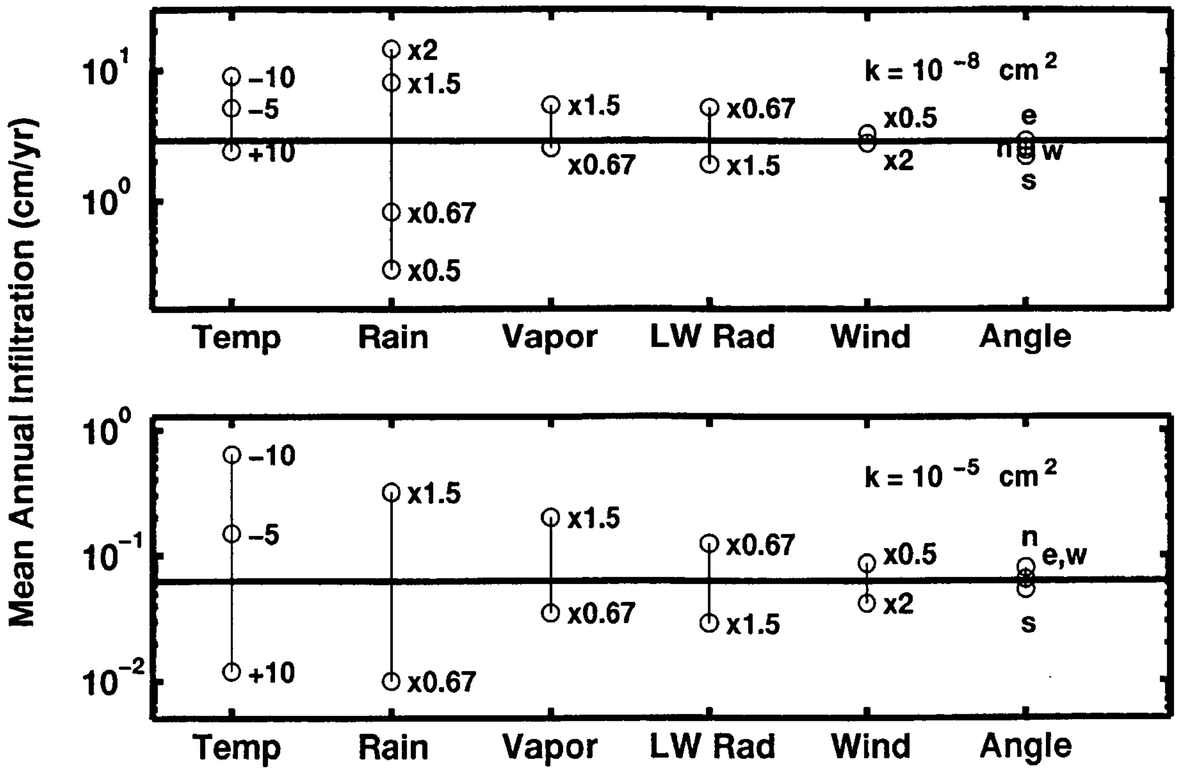

Figure 2: Long-term net bare-soil infiltration for two semi-infinite alluvium columns with different k, and with uniformly perturbed meteorological parameters.

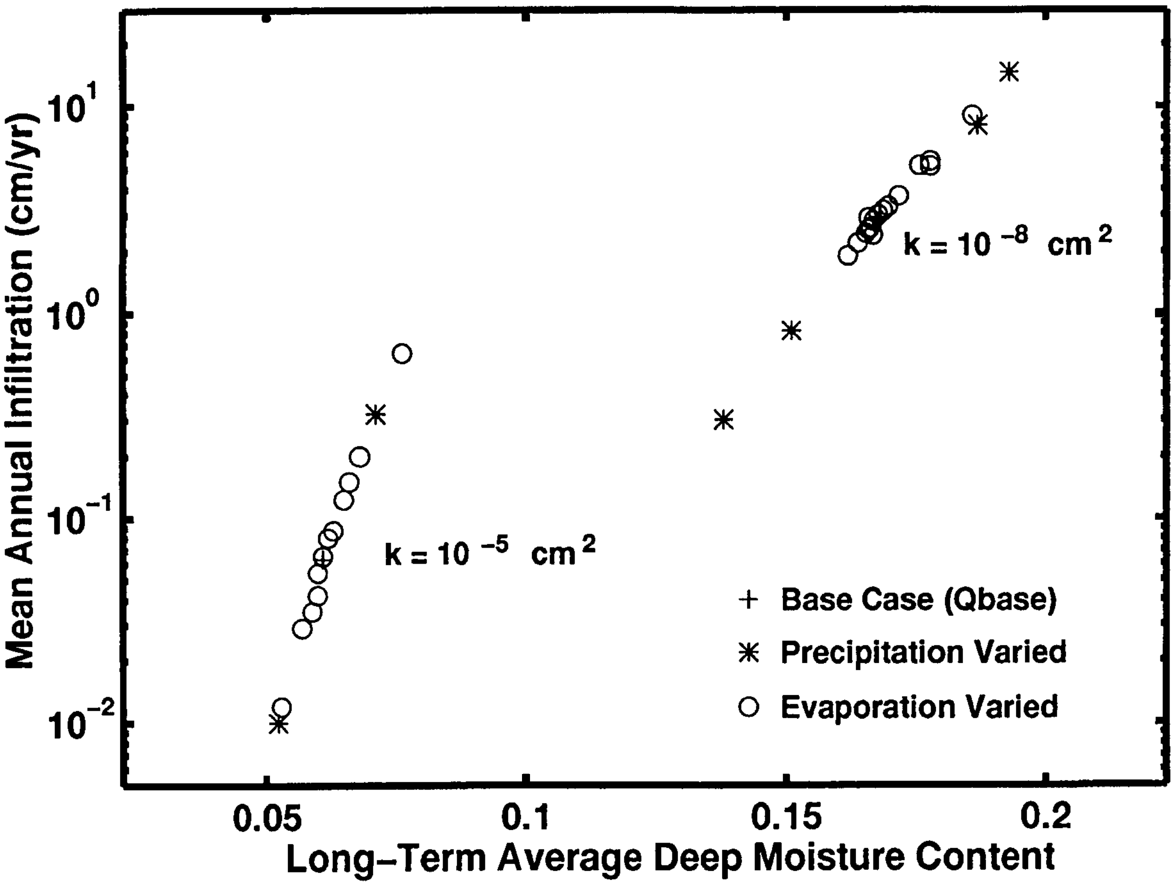

Figure 3: Changes to long-term net bare-soil infiltration in two semi-infinite columns due to systematic change in meteorological parameters.

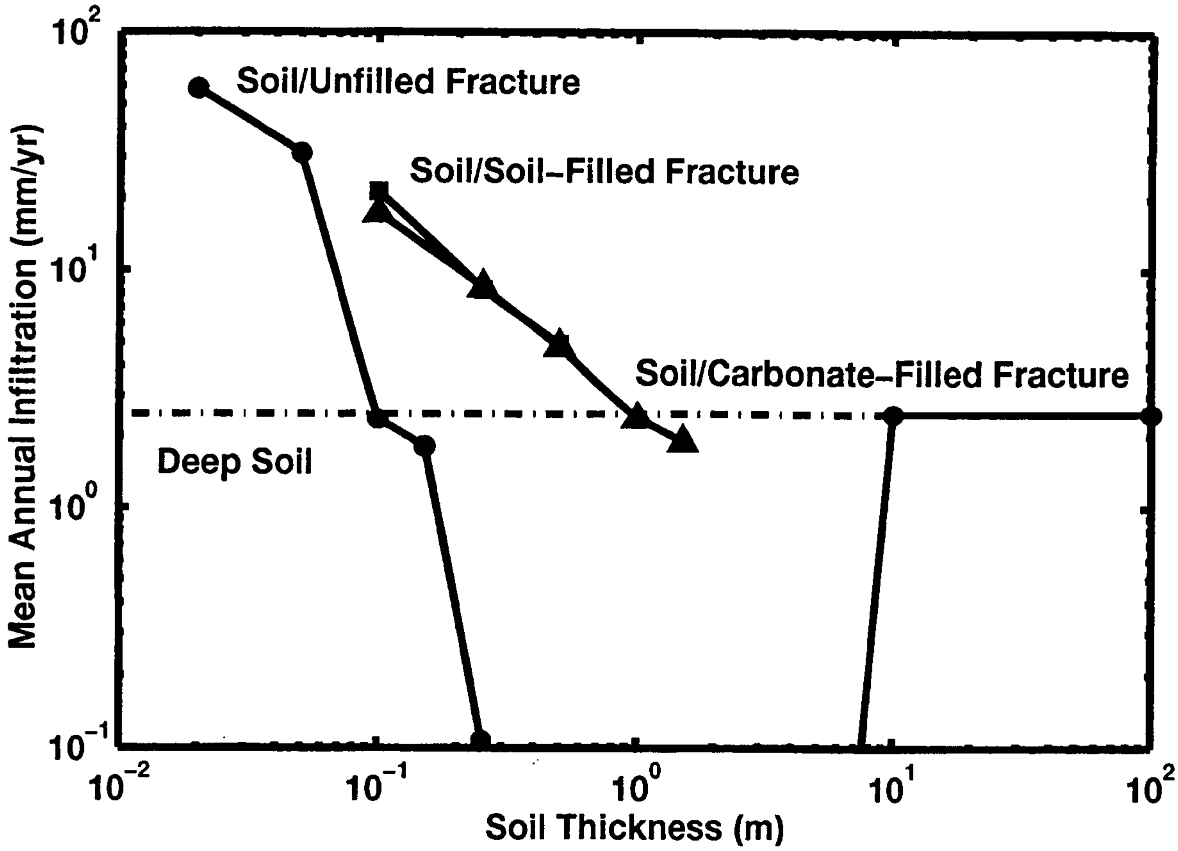

Figure 4: Typical response of bare-soil MAI simulations to soil thickness when fractures are unfilled, soil-filled, or carbonate-filled. The bare-soil MAI for a semi-infinite soil column is shown for reference.

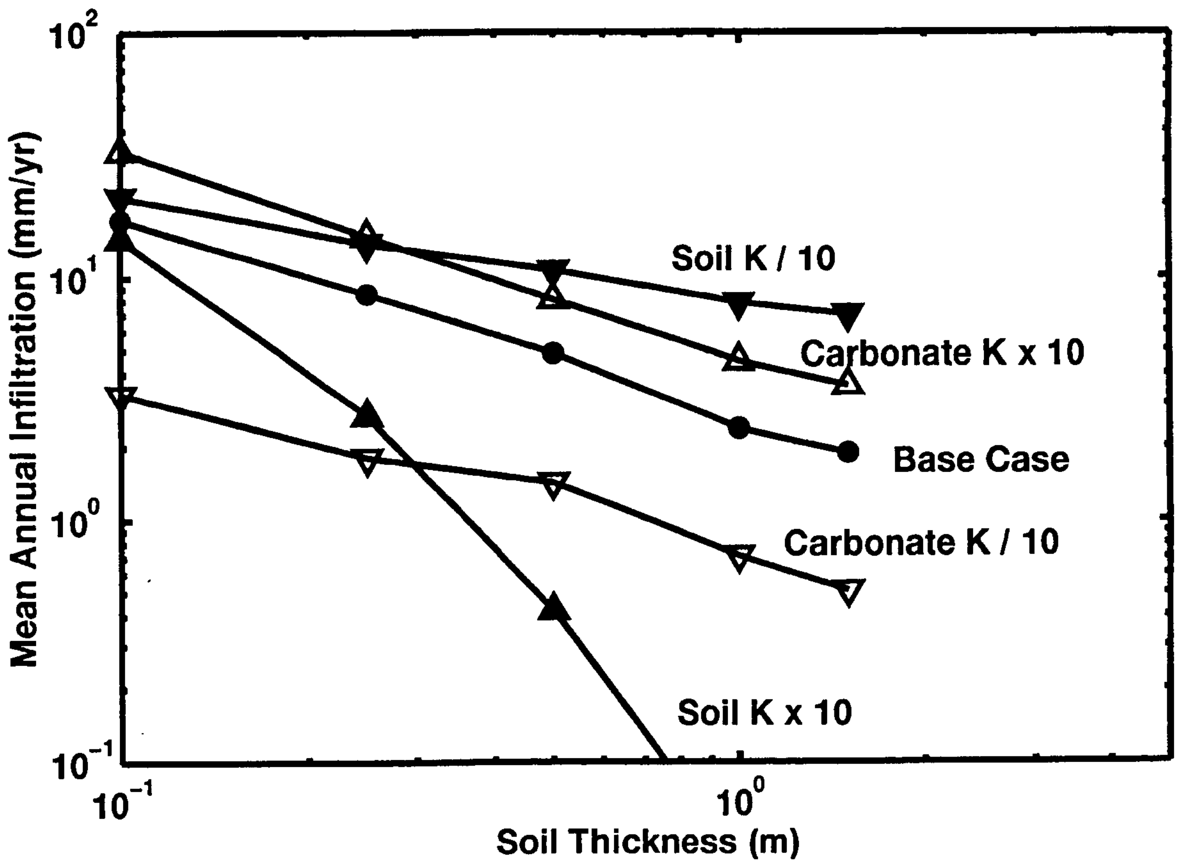

Figure 5: Typical response of MAI simulations to soil and fracture hydraulic properties for bare soil above a carbonate-filled fracture system.

38/45

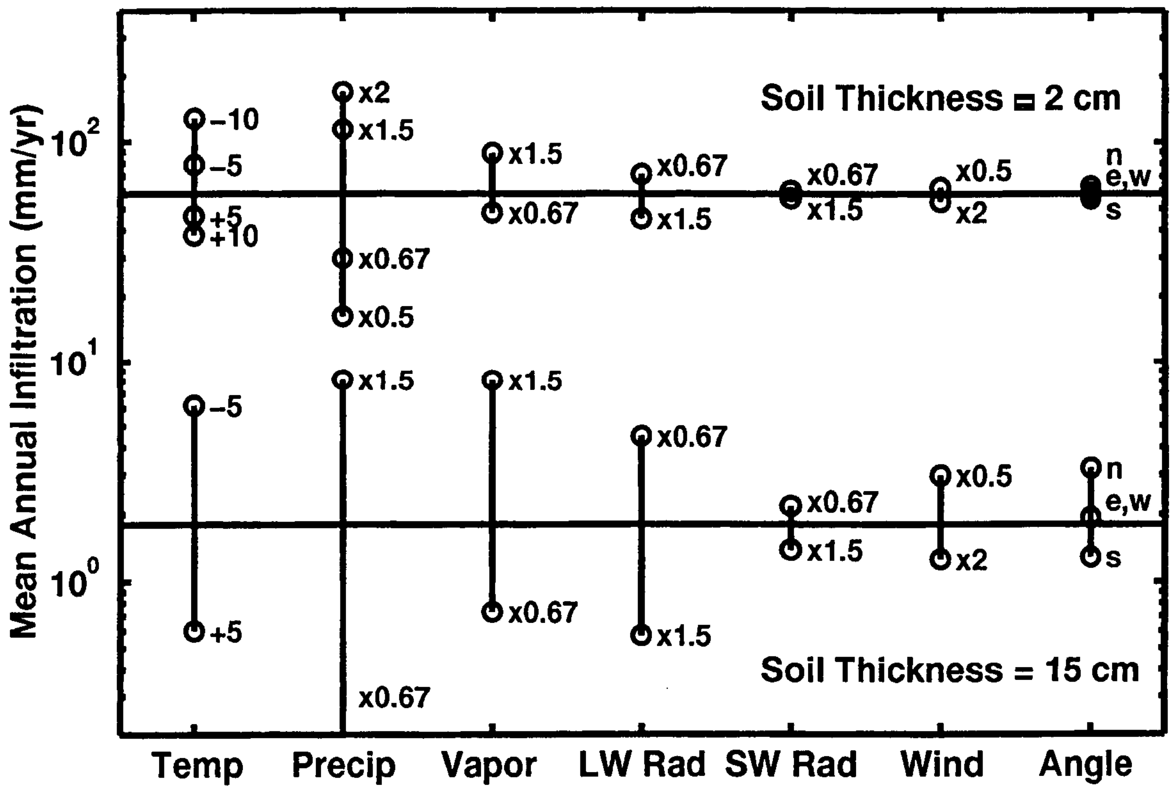

Figure 6: Typical response of MAI simulations to meteorologic factors for 2 and 15 cm of bare soil above an unfilled fracture system.

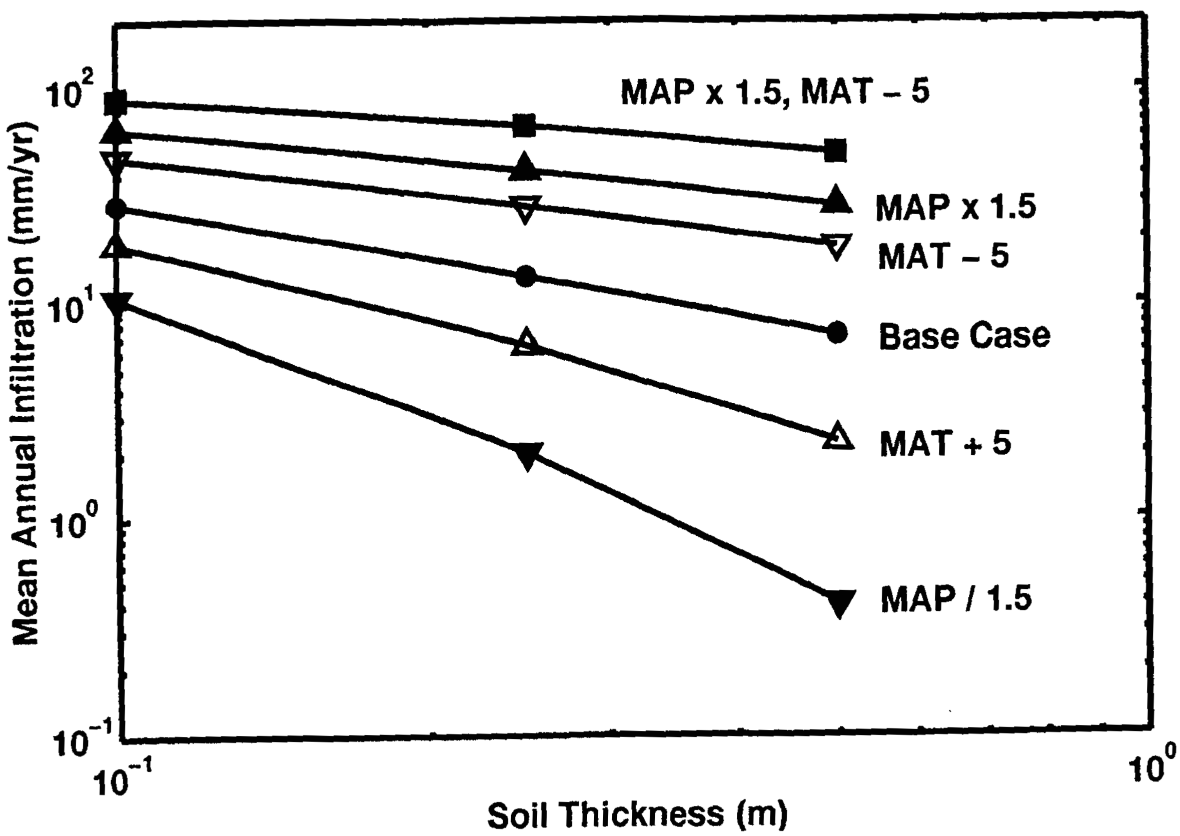

Figure 7: Typical response of MAI simulations to MAP and MAT for bare soil above a carbonate-filled fracture system.

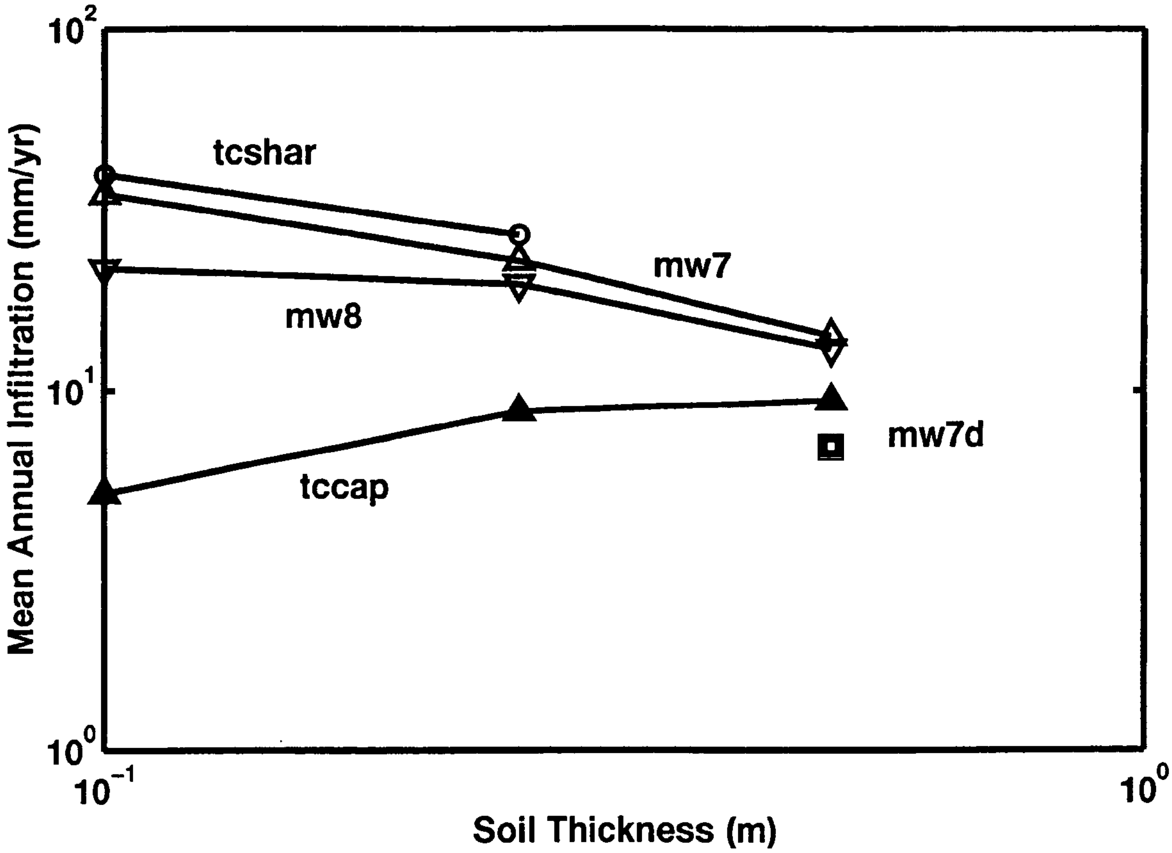

Figure 8: Typical response of MAI simulations to bedrock hydraulic properties for bare soil above an unfractured tuff bedrock. Note that using daily meteorologic inputs can result in systematic underprediction of MAI relative to hourly inputs (mw7 versus mw7d).

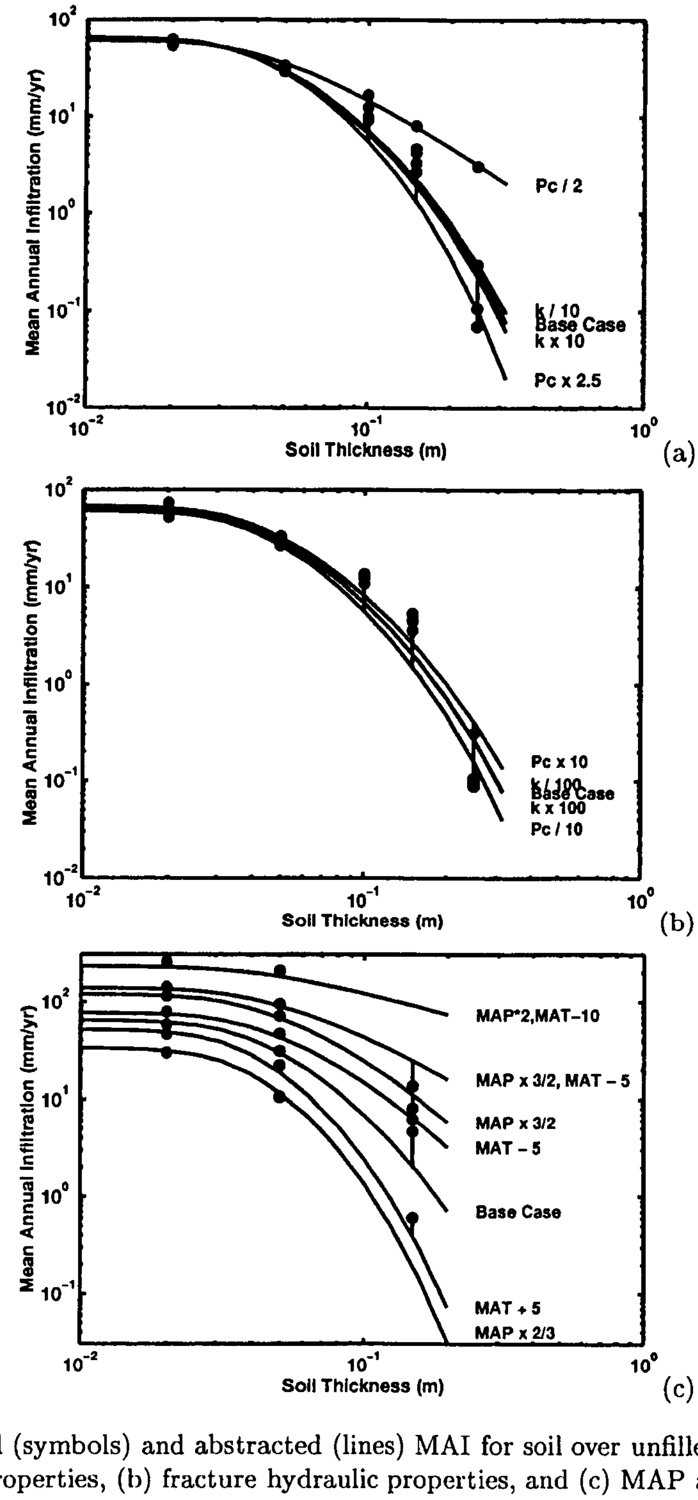

Figure 9: Simulated (symbols) and abstracted (lines) MAI for soil over unfilled fractures, varying: (a) soil hydraulic properties, (b) fracture hydraulic properties, and (c) MAP and MAT.

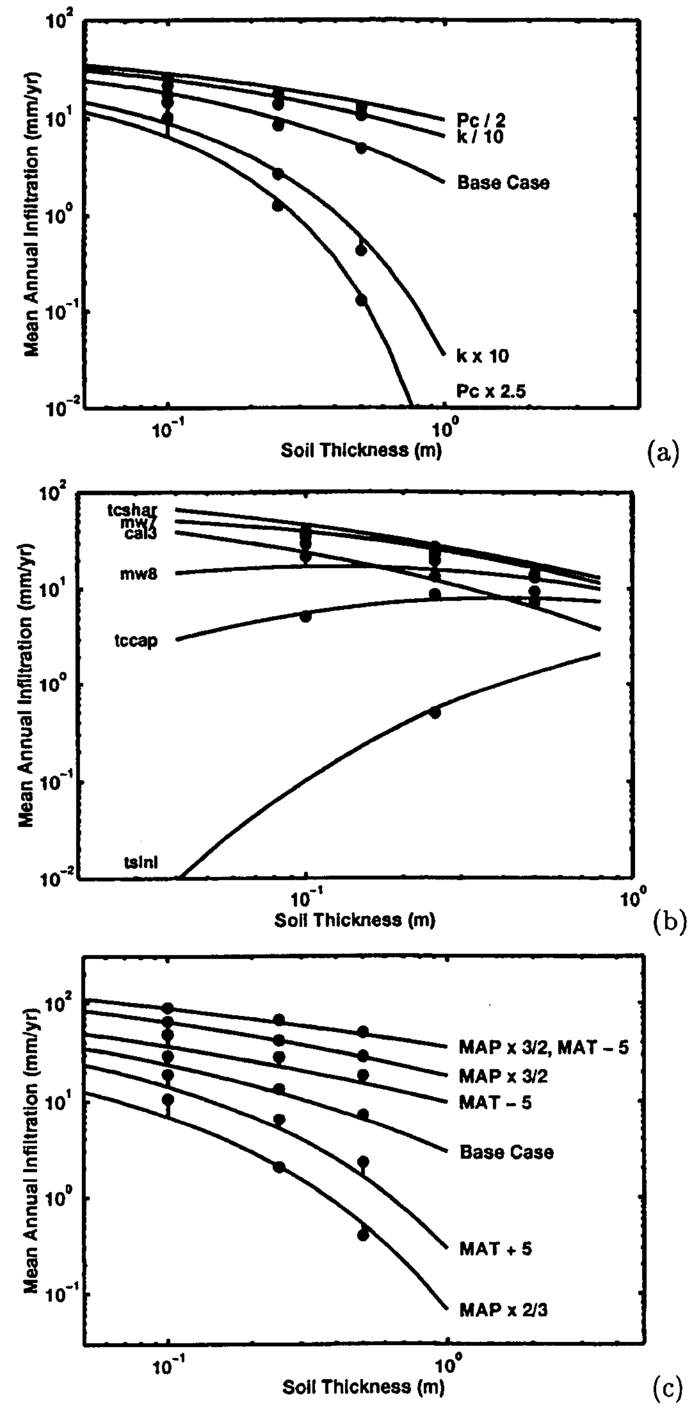

Figure 10: Simulated (symbols) and abstracted (lines) MAI for soil over (a) carbonate, with various soil properties; (b) typical bedrock, and (c) carbonate, varying MAP and MAT.

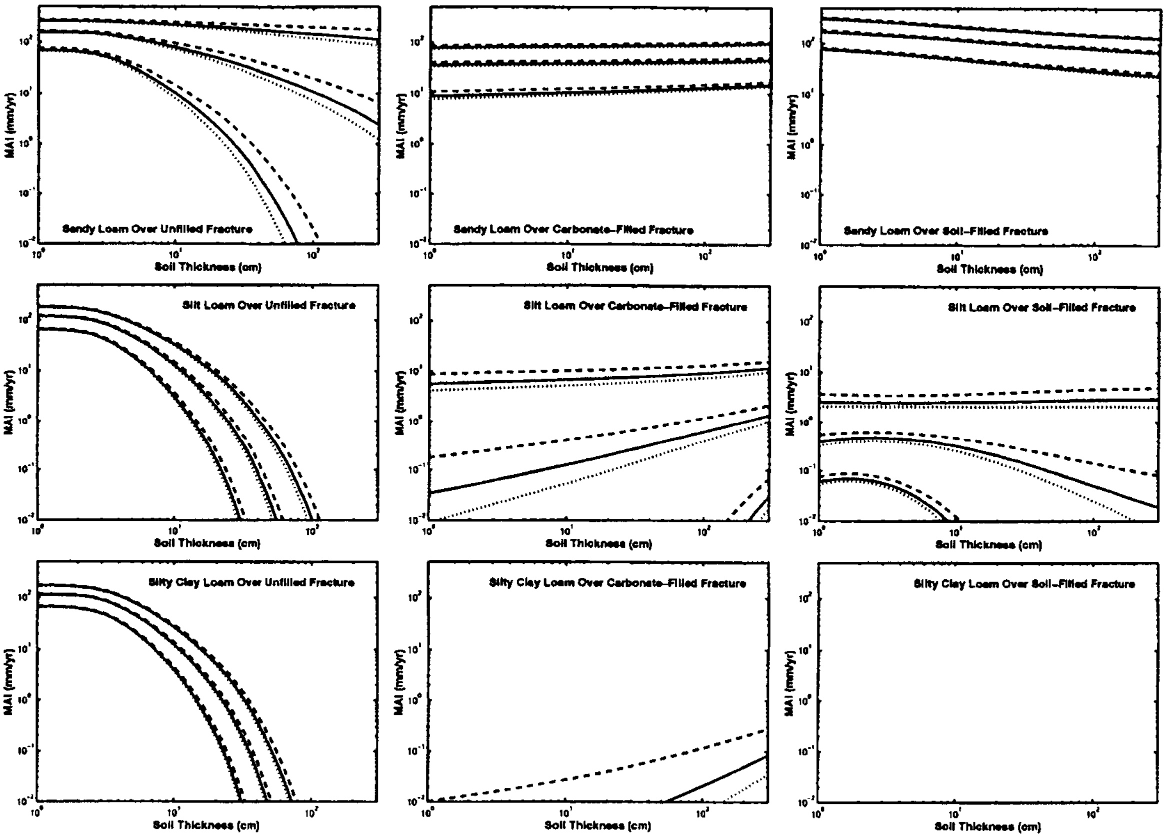

Figure 11: Abstracted MAI for a soil over unfilled, carbonate-filled, or soil-filled fractures. Each plot has predictions at 1300, 1900, and 2400 m (increasing elevation increases MAI). For each elevation, south-, upward-, and north-facing slopes are denoted by dotted, solid, and dashed lines, respectively. Note that MAI for silty clay loam over soil-filled fractures is essentially zero.

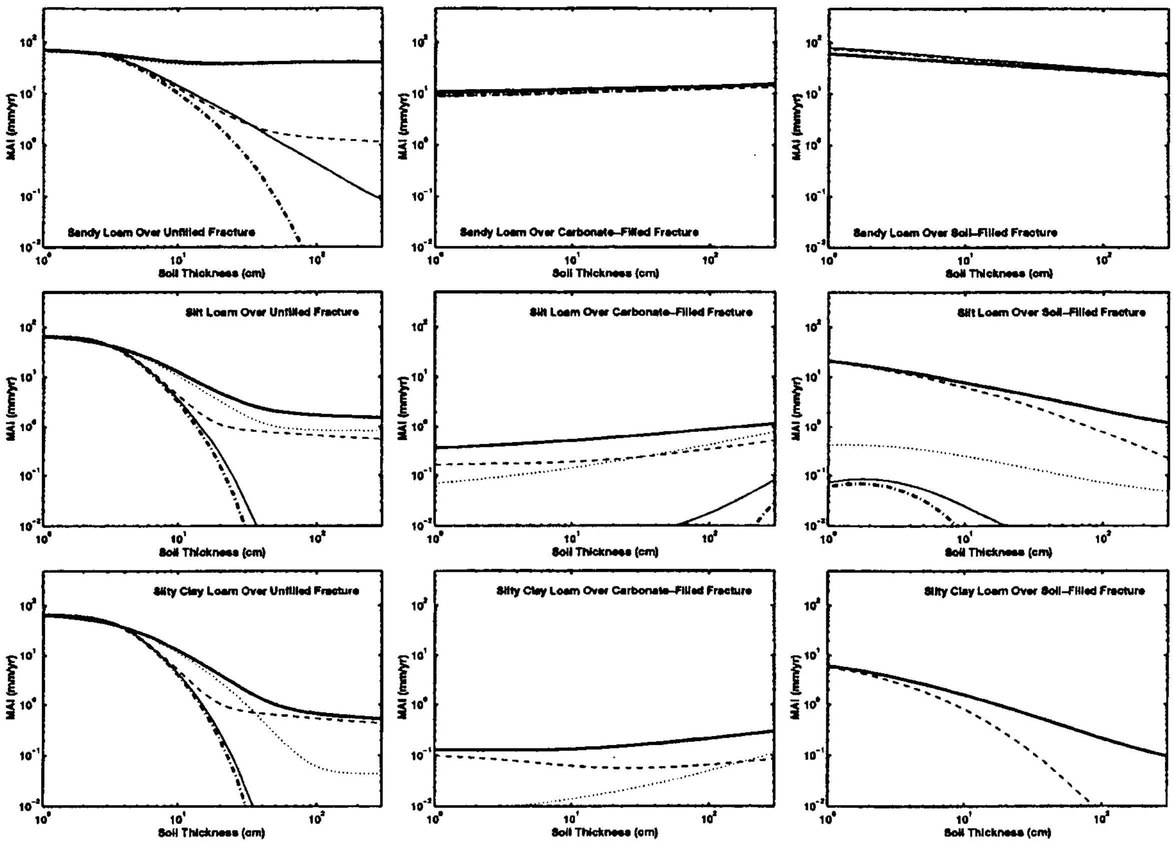

Figure 12: Abstracted MAI for a soil over unfilled, carbonate-filled, or soil-filled fractures at 1300 m. Unperturbed and fully perturbed cases are represented by heavier lines (dash-dot and solid lines, respectively). Lighter lines represent cases with only soil, fracture, or climate inputs perturbed (dotted, dashed, and solid lines, respectively).

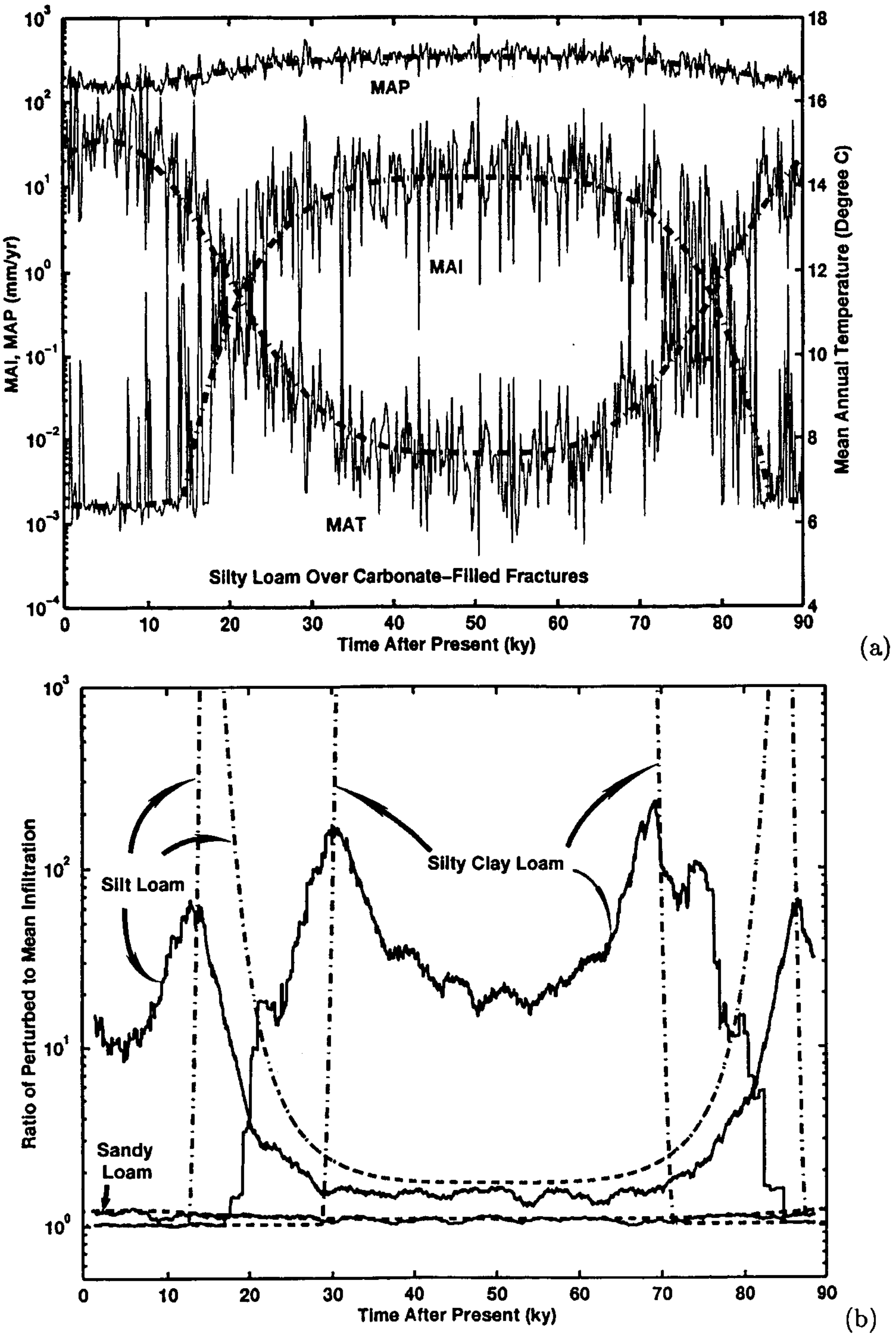

Figure 13: For 30-cm-thick soil, (a) mean and perturbed MAP, MAT, and bare-soil MAI over an abstracted glacial cycle using silty loam; and (b) the ratio of expected and moving-average perturbed MAI to MAI for mean MAP and MAT (Monte-Carlo predictions use solid lines while first-order predictions use dashed lines).